Expression patterns of FGF and BMP pathway genes in the tardigrade *Hypsibius exemplaris*

Kira L. Heikes[1,2] and Bob Goldstein[1,2,3,*]

[1] Biology Department, University of North Carolina at Chapel Hill, Chapel Hill, NC, USA

[2] Curriculum in Genetics and Molecular Biology, University of North Carolina at Chapel Hill, Chapel Hill, NC, USA

[3] Lineberger Comprehensive Cancer Center, University of North Carolina at Chapel Hill, Chapel Hill, NC, USA

[*] Corresponding author: Department of Biology, University of North Carolina at Chapel Hill, 616 Fordham Hall, Campus Box 3280, Chapel Hill, NC 27599-3280
E-mail: bobg@unc.edu

Abstract

A small number of conserved signaling pathways regulate development of most animals, yet we do not know where these pathways are deployed in most embryos. This includes tardigrades, a phylum with a unique body shape. We examined expression patterns of components of the BMP and FGF signaling pathways during embryonic segmentation and mesoderm development of the tardigrade *Hypsibius exemplaris*. Among the patterns examined, we found that an FGF ligand gene is expressed in ectodermal segment posteriors and an FGF receptor gene is expressed in underlying endomesodermal pouches, suggesting possible FGF signaling between these developing germ layers. We found that a BMP ligand gene is expressed in lateral ectoderm and dorsolateral bands along segment posteriors, while the BMP antagonist Sog gene is expressed in lateral ectoderm and also in a subset of endomesodermal cells, suggesting a possible role of BMP signaling in dorsal-ventral patterning of lateral ectoderm. In combination with known roles of these pathways during development of common model systems, we developed hypotheses for how the BMP and FGF pathways might regulate embryo segmentation and mesoderm formation of the tardigrade *H. exemplaris*. These results identify the expression patterns of genes from two conserved signaling pathways for the first time in the tardigrade phylum.

Keywords

Tardigrades, BMP, FGF, Segmentation, Mesoderm

Introduction

Embryonic development relies on precise temporal and spatial patterning for formation of the correct body shape. Organisms come in many unique forms, as the result of unique developmental trajectories, yet each trajectory involves widely conserved cell signaling pathways (Pires-daSilva and Sommer, 2003). Among animals, these include the FGF, BMP, Wnt, Hedgehog, Hippo, and Delta-Notch signaling

pathways (Pires-daSilva and Sommer, 2003). There is a breadth of knowledge about how cell signaling refines developmental patterns in common model organisms, such as fruit flies, nematodes, mice, frogs, and zebrafish (Pires-daSilva and Sommer, 2003). Much less is known about how cell signaling facilitates the formation of other unique body forms (Martinez, 2018).

Tardigrades comprise an entire phylum of animals whose development is little studied. Tardigrades are well positioned for studying the evolution of development of diverse organisms, as they are members of the diversely shaped ecdysozoan animals, a clade that also includes arthropods and nematodes (Aguinaldo et al., 1997; Gabriel et al., 2007; Smith et al., 2023). Tardigrades exhibit a body plan consisting of a head with two eyes and four leg-bearing trunk segments (reviewed in Schill, 2018). One species of tardigrade, *Hypsibius exemplaris*, is an emerging model system, with established methods for *in situ* hybridization to visualize gene expression patterns (Gabriel et al., 2007; Goldstein, 2022a, 2022b, 2018; Goldstein and Blaxter, 2002; Smith et al., 2016). Homology of major body regions of *H. exemplaris* embryos has been explored through the lens of Hox gene expression patterns (Smith et al., 2016). Patterning has been explored by studying proximal-distal leg patterning genes, nervous system patterning genes, and Engrailed and Pax3/7 (Gabriel and Goldstein, 2007; Game and Smith, 2020; Smith et al., 2023, 2018).

Additional positional information from cell signaling likely contributes to specify the location, size, and morphology of tissue folds, organs, and appendages during development of this unique body form. Various Wnt ligands exhibit non-overlapping mRNA expression in *H. exemplaris* (Chavarria et al., 2021). Using *in situ* hybridization to observe where and when Wnt ligand mRNAs were expressed, the study authors hypothesized potential roles of Wnt signaling in *H. exemplaris* development and theorized that loss of many Wnt signaling pathway components, as well as the non-overlapping expression patterns of ligands, contributed to the evolution of the miniaturized tardigrade body. Where and when other conserved cell signaling pathways are deployed in tardigrade embryos have yet to be revealed. Here, we reveal the expression of genes in two major pathways, FGF (Fibroblast Growth Factor) and BMP (Bone Morphogenetic Protein), during development of the tardigrade *H. exemplaris*.

We focus on the FGF and BMP pathways, in part because these pathways frequently intersect to refine development. In *Danio rerio* and *Mus musculus*, BMP and FGF, expressed in different regions of the embryo, pattern developing mesoderm (Row et al., 2018). There is also intracellular cross-talk between these pathways and their transcriptional targets: BMP can activate a transcription factor family that antagonizes a different, FGF-activated transcription factor family (Luo, 2017; Row et al., 2018). In *Drosophila melanogaster*, FGF ligands activate *sog* (BMP antagonist) and repress *dpp* (BMP ligand) expression (Stathopoulos et al., 2004). In the spider *Parasteatoda tepidariorum*, FGF signaling affects BMP signaling downstream of BMP ligand, as mutants for FGF receptor lead to significant reduction in phosphorylated SMAD, a readout of active BMP signaling (Wang et al., 2023).

FGF signaling has known roles in regulating body segmentation patterning and mesoderm development across animals (Muha and Müller, 2013). BMP signaling has known roles in regulating early dorsal-ventral patterning, mesoderm differentiation, primordial germ cell development, and appendage patterning across animals

(Donoughe et al., 2014; Nakayama et al., 2000; Ramel and Hill, 2012; Winnier et al., 1995). Previous studies that take advantage of conservation of FGF and BMP signaling have made comparisons between vertebrate and invertebrate systems, which has proven fruitful in expanding mechanistic understanding of these pathways (Huang and Stern, 2005). Broadening this to non-model systems will contribute to understanding how differential deployment of FGF and BMP signaling leads to morphogenesis of diverse tissue and animal shapes (Matus et al., 2007; Rentzsch et al., 2008).

Expression patterns of pathway components often provide a clue as to their role in development. Approaches based entirely on RNAseq data compare expression dynamics of regulatory genes to reveal novel insights into embryonic development (Levin et al., 2016; Tu et al., 2014). Using a staining approach, such as *in situ* hybridization, adds spatial context to this temporal information. We deployed *in situ* hybridization to examine the expression patterns of components of the FGF and BMP signaling pathways during segmentation of *H. exemplaris* embryos. We describe the observed expression patterns in the Results below. Based on these observed patterns and known roles in other animals, we present testable hypotheses about the potential roles of FGF and BMP signaling during tardigrade segmentation and mesoderm development.

Results

Identification of conserved signaling pathway genes in *H. exemplaris*

We identified homologs of upstream components of the FGF signaling pathway in *H. exemplaris* from RNAseq and genomic resources (Levin et al., 2016; Yoshida et al., 2017). Within this pathway, FGF ligands bind FGF receptor tyrosine kinases, leading to receptor dimerization and transphosphorylation, which activates intracellular cascades and transcriptional changes (Muha and Müller, 2013). We identified one FGF ligand homolog: FGF8 (Supp. Fig. 1) and two homologs of FGF receptors: FGFRL1 and FGFRL2 (FGF receptor-like 1 and 2, respectively, Supp. Fig. 2). Expression levels in a previously published embryonic transcriptome through *H. exemplaris* development suggested to us that FGFRL1 is expressed at high enough levels for detection by fluorescence *in situ* hybridization (FISH), but FGFRL2 is very weakly expressed (Levin et al., 2016). We concluded that FGFRL1 is likely to be a relevant receptor during embryonic development in *H. exemplaris* and moved forward with this gene to identify cells likely receptive to FGF signaling. The homolog of FGF8 was not captured in this staged transcriptome. We also identified a homolog of the mesodermal transcription factor Snail in the hopes of using it as a marker of embryonic mesoderm (Supp. Fig. 3), which was lowly expressed in the staged transcriptome (Levin et al., 2016).

We also identified homologs of components of the BMP signaling pathway in *H. exemplaris* (Levin et al., 2016). During signaling, BMP ligands bind Type I and II BMP serine/threonine kinase receptors, leading to receptor heterotetramer formation and phosphorylation of the Type I receptor by the Type II receptor, which triggers intracellular signaling and transcriptional changes (Ramel and Hill, 2012). Extracellular BMP ligands can be regulated by several other extracellular proteins (Nunes da Fonseca et al., 2010). The antagonist Short gastrulation (Sog)/Chordin binds collagen in the extracellular matrix and prevents BMP ligand from dispersing (Ashe and Levine, 1999; Holley et al., 1995; Sasai et al., 1994). The protease Tolloid (Tld) assists in releasing BMP ligand from Sog, by cleaving Sog protein (Mullins, 1998; Winstanley et

al., 2015). We found one homolog each of the BMP2/4-type ligand Dpp, the BMP5/6/7/8-type ligand Gbb (Supp. Fig. 4), the BMP antagonist Sog (Supp. Fig. 5), the Type 1 and Type 2 BMP receptors (Supp. Fig. 6) Tkv and Punt, the Type 1 BMP receptors Sax and Baboon, and the protease Tolloid (Supp. Fig. 7). We also identified one homolog each of known downstream transcriptional targets of BMP signaling as potential markers of active signaling, Dorsocross1 (Doc1) and Eyes Absent (Eya) (Supp. Fig. 8 and Supp. Fig. 9). Eyes Absent (Eya) is also known to be a target of FGF signaling (Ahrens and Schlosser, 2005). All of these identified homologs were highly expressed between elongation and segmentation stages in the published staged transcriptome (Levin et al., 2016).

We determined where each of these upstream signaling pathway genes is expressed during segmentation of *H. exemplaris* embryos using FISH. Although mRNA distributions are affected by mRNA synthesis, localization, persistence, and depletion, we refer to the presence of mRNA, detected by FISH, as gene expression for simplicity. A summary of the relevant embryonic stages is presented in Fig. 1.

By ectodermal segmentation, FGF ligand *fgf8* is expressed in segmentally iterated patches of ectodermal cells and FGF receptor *fgfrl1* is expressed in underlying endomesodermal pouches.

To simultaneously detect where the FGF ligand *fgf8* and the FGF receptor *fgfrl1* are expressed at a post-ectodermal segmentation stage, 24 hours post laying (hpl), we applied double FISH. We found that *fgf8* was expressed in a segmentally iterated pattern in the ectoderm – in patches of lateral ectodermal cells in the posterior of each trunk segment on both the left and right sides of embryos (Fig. 2 and Video 1). Additional patches of *fgf8* expression were seen laterally near the middle of the head segment in ectoderm and in a small set of cells at the posterior of the head segment in ectoderm and endomesoderm (Fig. 2). While *fgf8* was expressed in a segmentally repeating pattern in the ectoderm, *fgfrl1* was expressed in the endomesodermal pouches found within each of the four trunk segments, in the developing foregut in the head segment, and to a lesser extent in the ectoderm (Fig. 2 and Video 2). The segmentally-iterated patches of *fgf8* led us to wonder when these patches emerge relative to the timing of body segmentation.

Segmentally iterated *fgf8* expression begins prior to ectodermal segmentation and near the time when endomesodermal pouches form.

To determine if segmentally iterated *fgf8* expression preceded or followed body segmentation, we detected expression at earlier stages – at late elongation (~18 and 19 hpl), endomesodermal pouch formation (~20 hpl), and ectodermal segmentation (~21-22 hpl), corresponding to stages 11-13 from previous publications (Chavarria et al., 2021; Gabriel et al., 2007). Between 18 hpl and 22 hpl, the expression pattern of *fgfrl1* did not change dramatically and was enriched mostly in endomesodermal cells. In contrast, the expression pattern of *fgf8* evolved. At elongation stages, there were fewer, broad patches of *fgf8* expression than at later stages (Fig. 3 A-A’’’ and Supp. Fig. 10). Following ectodermal segmentation (~21-22 hpl), ectodermal patches of *fgf8* expression began to resemble what we saw at 24 hpl, i.e. segmentally iterated, in lateral pairs in the posterior of each trunk segment and in the middle of the head segment, in addition to being in a small group of cells in the posterior of the head segment (Fig. 3 C-C’’’ and D-D’’’). Ectodermal segmentation is evident by the presence of furrows in the ectoderm

at the approximate boundaries between body segments (Fig. 1) (Chavarria et al., 2021; Gabriel et al., 2007; Gabriel and Goldstein, 2007). At 20 hpl, when endomesodermal pouches have formed but ectodermal segmentation has not occurred, patches of *fgf8* expression were present in the lateral ectoderm on each side of the embryo (Fig. 3 B-B'''). This expression pattern reveals that enrichment of *fgf8* in the ectoderm of each segment precedes apparent ectodermal segmentation of the embryo and either follows or occurs concomitantly with endomesodermal pouch formation.

The patches of *fgf8* expression also appeared to change in orientation relative to the axes of the embryo. Upon ectodermal segmentation, the patches were positioned in cells in the posterior of each segment and perpendicular to the anterior-posterior axis (Fig. 2 and Fig. 3 C and D). Prior to ectodermal segmentation, the patches were positioned parallel to the anterior-posterior axis, occurring along the segments (Fig. 3 B). Therefore, the pattern of *fgf8* is dynamic during the morphological process that leads to ectodermal segmentation of the embryo.

The mesodermal transcription factor *snail* is expressed in non-mesodermal cells.

To determine more precisely which cells in endomesodermal pouches contribute to the mesoderm, we detected expression for the ectodermal transcriptional repressor *snail*, which historically serves as a marker of mesodermal fate in animal embryos, together with the pro-mesodermal transcription factor *twist* (Leptin, 1991). However, *snail* was expressed throughout the embryo, in both ectodermal and endomesodermal layers of cells at both elongation and ectodermal segmentation stages (Fig. 4). Expression of *snail* appeared to become more enriched in the internal endomesodermal cells by 24 hpl but was still present in ectodermal cells (Fig. 4 A-D). Therefore, *snail* expression is not a reliable marker of mesodermal fate at this stage in development. By double FISH, *snail* was expressed in cells that expressed *fgfrl1* (Fig. 4 A-A''' and B-B''') and in cells that expressed *fgf8* (Fig. 4 C-C''' and D-D'''). Given this overlap, and the lack of overlap between *fgf8* and *fgfrl1* expression revealed above in Fig. 2, this expression pattern suggests that *snail* is expressed in both FGF sending and FGF receiving cells.

Based on all of the results examining expression of FGF pathway genes, we conclude that the ligand-encoding gene *fgf8* is expressed primarily in lateral ectoderm in the posterior of each body segment, as well as in the head, and the receptor-encoding gene *fgfrl1* is expressed broadly, enriched in endomesoderm underlying the ectoderm.

BMP ligand *dpp* and antagonist *sog* are expressed in lateral ectoderm, and *dpp* is expressed more dorsally than *sog*

To determine where components of the BMP signaling pathway are expressed at the ectodermal segmentation stage, we detected expression of BMP receptor *tkv* and *punt*, BMP ligands *dpp* and *gbb*, BMP antagonist *sog*, and Sog-cleaving protease *tld*. Receptors *tkv* and *punt* were ubiquitously expressed across the embryo (Supp. Fig. 11). The ligand *gbb* was also ubiquitously expressed throughout the embryo (Supp. Fig. 12). However, *gbb* expression appeared to be absent from the cells previously defined as the primordial germ cells, whereas receptors *tkv* and *punt* were expressed in the primordial germ cells (Heikes et al., 2023).

By double FISH, the ligand *dpp* and the antagonist *sog* were expressed in ventro-lateral ectoderm (Fig. 5 and Video 3). Neither gene was expressed on the most dorsal surface of the embryo (Fig. 5 C and Video 4). *dpp* was expressed in more dorsal

regions of lateral surfaces than *sog* (Fig. 5 C). At the anterior-most tip of the head where the mouth likely develops, *sog* was expressed in bands on either side but did not appear to be expressed in the epithelium of the developing foregut (Marcus, 1929) (Fig. 5 A and B). *dpp* was expressed in large patches of ectodermal cells overlapping and dorsally adjacent to these two bands of cells enriched for *sog* (Fig. 5 A and B). *sog* was also expressed in one endomesodermal cell on the ventral side of each of the endomesodermal pouches in each body segment (Fig. 5 D). *dpp* was expressed in bands extending over each segment near the segment boundaries (Fig. 5 C and D). These bands were in the overlying ectoderm adjacent to the endomesodermal cells that expressed *sog*. We wondered whether these regions of *dpp* and *sog* expression preceded or coincided with the segmentation of the ectoderm and/or endomesoderm.

We compared expression of *dpp* and *sog* by double FISH at key stages: elongation (18 and 19 hpl), endomesodermal pouch formation (20 hpl), and ectodermal segmentation (21 hpl). Lateral expression of *dpp* and *sog* were apparent by elongation (18 hpl) (Fig. 6 A). However, *dpp* was expressed in broader swaths of lateral ectoderm at elongation than at segmentation stages, and *sog* was expressed in a shorter region along the A-P axis of lateral ectoderm at elongation than at segmentation stages (Fig. 6 A-B vs C-D). Bands of *dpp* either coincided with or followed ectodermal segmentation (Fig. 6 D), and endomesodermal cells began expressing *sog* after endomesodermal pouch formation and during or after ectodermal segmentation (Fig. 6 C-D). Antero-lateral bands of *sog* and *dpp* were apparent by elongation stages (18 hpl) (Fig. 6 A-B). These patterns indicate that *dpp* and *sog* are already expressed laterally prior to the processes of endomesodermal pouch formation and ectodermal segmentation and that the patterns of *dpp* and *sog* expression change throughout these morphological transformations.

Expression of the protease *tld* is increasingly restricted along the anterior-most end of the head from 19 to 24 hpl.

Having found *dpp* expression in lateral ectoderm and in bands near segment boundaries and antagonist *sog* expression in a more ventrally restricted domain of lateral ectoderm than *dpp*, we wondered where mRNA of the Sog protein-cleaving protease Tld was expressed. At elongation (19 hpl), *tld* was expressed in a wide band of cells along the anterior-most end of the head (Fig. 7 A). This band was mostly non-overlapping with the bands of *sog* expression that run on either side of the developing mouth (Fig. 5, Fig. 6, and Fig. 7 A) By endomesodermal pouch formation (20 hpl), the band of cells that expressed *tld* was thinner than at 19 hpl, indicating that *tld* expression becomes more restricted and/or that the *tld*-expressing cells condense in space between these stages (Fig. 7 B). This band of *tld* persisted through ectodermal segmentation (24 hpl) and remained mostly non-overlapping with the two bands of *sog* expression on either side (Fig. 7 C). At ectodermal segmentation stage, *tld* expression was mostly non-overlapping with the antero-lateral patches of cells that expressed *dpp*, which were located adjacent to and slightly overlapping with the bands of *sog* expression (Fig. 7 D and Fig. 5 and Fig. 6). *tld* did not appear to be expressed in the epithelium of the developing foregut (Fig. 7 C and D). These patterns indicate that *tld* is expressed in the cells where the mouth likely develops, surrounded on either side by cells that express *sog* and *dpp*.

Based on all of the results examining expression of BMP pathway genes, we conclude that the ligand-encoding gene *dpp* is expressed primarily in lateral ectoderm and in bands at posterior segment boundaries, as well as in the head, and the BMP antagonist-encoding gene *sog* is also expressed in lateral ectoderm, less dorsal than *dpp*, including the head, where two bands of *sog*-expressing cells are positioned between bands of *dpp*-expressing cells and an anterior band of cells expressing the protease *tld*.

The expression patterns of *doc1*, *eya*, and *dpp* after segmentation of *H. exemplaris* embryos.

These expression patterns left us wondering where BMP and FGF ligands are active during *H. exemplaris* segmentation. We turned to conserved downstream transcriptional targets of these pathways, *doc1* and *eya,* as likely markers of active signaling. *doc1* and *eya* are conserved targets of BMP signaling in other systems, such as *D. melanogaster* (Dominguez et al., 2016). Additionally, *eya* is known to be a target of FGF signaling (Ahrens and Schlosser, 2005). At ectodermal segmentation (24 hpl), *doc1* was expressed in ectoderm along the dorsal midline of the embryo, running in a band from the posterior tip of the embryo to the top of the head and then spreading into a larger region that did not extend to the anterior tip of the head (Fig. 8 A and B). *doc1* was mostly absent from internal germ layers. At ectodermal segmentation (24 hpl), hpl), *eya* was expressed in endomesodermal cells and almost entirely absent from ectoderm (Fig. 8 C and D). Expression of both *doc1* and *eya* appeared non-overlapping with the lateral ectoderm expression of *dpp* (Fig. 8). The expression of *eya* primarily in endomesoderm matches the pattern of *fgfrl1*-expressing cells that are likely receptive to FGF signaling.

Discussion

Here we reported the expression patterns of components of the FGF and BMP signaling pathways during development of the tardigrade *H. exemplaris* (summarized in Fig. 9). We found that FGF ligand *fgf8* and receptor *fgfrl1* are expressed in different germ layers of embryos between elongation and ectodermal segmentation stages. *fgf8* is expressed in ectoderm at segment posteriors, and *fgfrl1* is expressed in underlying endomesoderm. The segmental expression pattern of *fgf8* precedes visible signs of ectodermal segmentation and arises around or concurrently with endomesodermal pouch formation. We also found that BMP ligand *dpp* and antagonist *sog* are both expressed laterally and that *dpp* is expressed more dorsally than *sog*. Additionally, *sog* is expressed in bands of ectoderm on either side of the developing mouth, and *dpp* is expressed in patches slightly overlapping and adjacent to these bands of *sog* expression. These patterns are apparent by elongation stages and become more elaborate during the morphological process of segmentation.

What follows is a discussion of these observed expression patterns and hypotheses of the potential roles of FGF and BMP in *H. exemplaris* development. See Table 3 for a more comprehensive summary of all hypotheses. Testing these will rely on development of techniques not yet established for this system. Our attempts to use RNAi and chemical inhibitors to FGF (SU5402 and U0126) and BMP signaling (Dorsomorphin, DMH1, and LDN-212854) were unsuccessful (data not shown). Attempting to mark active FGF and BMP signaling, we also stained embryos using cross-reactive anti-pSMAD and anti-dpERK antibodies but did not detect specific signal (data not shown). There has been recent progress towards development of genetic tools for *H. exemplaris*

by CRISPR/Cas9-based genome editing of adults with 10-20% efficient genomic deletion and via a vector-based expression system that worked mosaically in adult cells at 70-89% adult transfection efficiency and rare germline transmission (Kumagai et al., 2022; Tanaka et al., 2022). Recently, there has been progress in another tardigrade species, *Ramazzottius varieornatus*, in which CRISPR injected directly into the maternal body cavity exhibited germline transmission with low efficiency (3-4%) (Kondo et al., 2024). We anticipate improvements to these techniques are soon to follow for efficient germline transmission, which would facilitate asking questions about development. Specifically, tools such as transcriptional reporters, as well as inducible protein regulation, will enable temporally specific tests of signaling pathway functions during key stages in development.

The changing pattern of *fgf8* between elongation and segmentation raises a few questions. First, how are patches of *fgf8* initiated? Second, how are more patches of *fgf8* formed from the few detected? Third, what drives the change of *fgf8* patch orientation relative to the embryo's body axes? Additionally, based on their position and presence prior to ectodermal segmentation, we further speculate that *fgf8*-expressing cells might play a role in ectodermal furrowing.

The non-overlapping enrichment of *fgf8* and *fgfrl1* is consistent with roles of FGF in other animal phyla: guidance of mesoderm migration, mesodermal fate commitment (in conjunction with BMP), and patterning of muscle body wall attachment sites. We speculate that FGF might serve these roles between elongation and segmentation. Additionally, FGF (in conjunction with Wnt) is known to play a role in posterior segment polarity and posterior somite formation in chordates. Although in protostome animals studied so far only Wnt appears to be involved in posterior segment polarity and FGF does not, tardigrades may break this rule. If this is the case, then endomesodermal pouch formation might follow *fgf8* mRNA patch formation (something we were not able to resolve with *in situs* that reveal still shots in developmental time). Related, another study found by antibody staining that Engrailed protein, which is also expressed in segment posteriors, follows formation of endomesodermal pouches and precedes ectodermal segmentation (Gabriel and Goldstein, 2007). Therefore, FGF8 could be an instructive cue for Engrailed expression, further reinforcing the posterior boundary of segments. The role of FGF in development has only been studied in a handful of protostome animals (Andrikou and Hejnol, 2021; Birnbaum et al., 2005; Huang and Stern, 2005; Lo et al., 2010; Sharma et al., 2015, 2013; Stathopoulos et al., 2004; Wang et al., 2023). If tardigrades (and other protostomes) employ FGF to pattern body segments, then this suggests the last common ancestor to deuterostomes and protostomes may have used FGF to pattern a segmental entity or that this role convergently evolved multiple times, perhaps due to the effectiveness of FGF at patterning iterative structures. Exploring FGF's role during development in additional protostome species is needed to address these possibilities.

The observation that *dpp* mRNA is enriched dorsally relative to its antagonist *sog* in tardigrades (a protostome phylum) is consistent with the role of BMP in regulating dorsal-ventral patterning in other animals (Morisato and Anderson, 1995). In other protostomes studied, BMP promotes dorsal fate, whereas in some deuterostomes studied, BMP promotes ventral fate, data that supports the dorsal-ventral inversion hypothesis (Arendt and Nubler-Jung, 1994; Holley et al., 1995). From the expression

patterns observed, we hypothesize that BMP regulates dorsal-ventral patterning of lateral ectoderm during the stages studied in *H. exemplaris*. BMP and its antagonist Sog are involved in symmetry breaking in certain contexts, as in the spider *Achaearanea tepidariorum* (Akiyama-Oda and Oda, 2006, 2003). Since symmetry breaking in the dorsal-ventral axis has already occurred by the stages of *H. exemplaris* development explored in this study, we hypothesize that BMP elaborates fates along the dorsal-ventral axis at these stages, as BMP is known to do in both protostomes and deuterostomes (Dale et al., 1992; Ferguson and Anderson, 1992; François et al., 1994; Holley et al., 1995; Jones et al., 1992; Sasai et al., 1994; Wharton et al., 1993).

Due to the banded expression pattern of *dpp* along each segment, we hypothesize that Dpp regulates the dorsal-ventral position of future limbs in each trunk segment, which aligns with a role of Dpp in regulating appendage formation in arthropods (Goto and Hayashi, 1997; Spencer et al., 1982). Alternatively or in addition, we hypothesize that Dpp regulates cuticle patterning by guiding cuticle deposition or sites of cuticle furrowing. The expression of *sog* on either side of the developing mouth led us to speculate that Dpp might provide signals inhibitory to mouth formation. Finally, due to the role of ectodermal BMP in regulating mesoderm development in *D. melanogaster*, *Danio rerio*, and *M. musculus*, among others, we hypothesize that Dpp regulates mesoderm development from overlying ectoderm (Frasch, 1995; Row et al., 2018; Staehllng-hampton et al., 1994).

In all hypotheses of Dpp function, Sog might act to restrict spread of Dpp ligand in one or multiple axes. This is complicated by the varying impacts that Sog/Chordin can have on BMP signaling and spreading (Nunes da Fonseca et al., 2010; Shimmi et al., 2005). Because of this, for all hypotheses, it is possible that Sog acts to facilitate further and directed spread of Dpp, in conjunction with Tld and Tsg (Nunes da Fonseca et al., 2010; Shimmi and O'Connor, 2003; Van Der Zee et al., 2006).

The protease Tld was expressed in a band where the mouth forms. Therefore, we speculate that, in conjunction with Sog, Tld might facilitate spreading and then release of Sog-bound Dpp either in the region of the developing mouth or internally to the mesodermal precursors in the endomesodermal pouches of cells surrounding the foregut. In addition, Tld is known to function in processing of collagens to mediate extracellular matrix (ECM) formation (Vadon-Le Goff et al., 2015). ECM has been shown to be important for pharyngeal morphogenesis in other animals, such as the nematode *Caenorhabditis elegans* (Rasmussen et al., 2012). Therefore, it is possible that in *H. exemplaris* embryos, Tld plays a role in pharyngeal development independent of BMP.

As mentioned, BMP ligand *gbb* was expressed throughout the embryo but excluded from the primordial germ cells, whereas BMP receptors *tkv* and *punt* were expressed throughout the embryo, including the primordial germ cells. This is consistent with the hypothesis that the primordial germ cells are receptive to BMP, which aligns with a known role of Gbb in regulating primordial germ cells in other systems (Donoughe et al., 2014; Lawson et al., 1999; Lochab and Extavour, 2017). Since *eya* was also expressed in the primordial germ cells, this suggests that *eya* may be a target of Gbb at this stage in development.

The expression pattern of *snail* was surprising, given that in other systems, Snail serves as a marker and promoter of mesoderm fate through inhibition of non-mesodermal genes (Alberga et al., 1991; Cano et al., 2000; Chopra and Levine, 2009;

Simpson, 1983). Although it does not appear to be a reliable marker of mesodermal fate at these stages in *H. exemplaris* development, the expression pattern of *snail* is potentially reflective of important aspects of mesodermal development in this system. It is possible that either mesoderm migrates from many starting points in development, including the ectoderm layer, or that many nonmesodermal cells express *snail* and only later in development is *snail* restricted to mesoderm.

Finally, between elongation and segmentation stages of *H. exemplaris* embryos, mesoderm forms. Given the known overlap of FGF and BMP in regulating mesoderm in other animals and given that these two pathways exhibit dynamic enrichment patterns between these stages, we speculate that FGF and BMP might work together to regulate proper mesodermal formation and/or fate specification (Row et al., 2018).

Conclusions:

Above, we present for the first time expression patterns for genes of components of the FGF and BMP signaling pathways during *H. exemplaris* development. The hypotheses we propose for how these pathways function will be testable upon development of new genetic tools in *H. exemplaris*. These results are timely, given the recent advances in and future potential of genetic tools in tardigrades. Understanding how cell signaling regulates the development of the unique tardigrade body plan will provide new information about how these conserved pathways regulate development of diverse tissue and organismal forms and ultimately how diverse body forms evolved through varied deployment of conserved cell signaling pathways.

Materials and Methods

Maintaining cultures of *Hypsibius exemplaris*

Cultures were maintained as described previously (Heikes et al., 2023; Mcnuff, 2018).

DIC imaging of development

DIC microscopy of embryonic development was performed as previously described (Heikes et al., 2023; Heikes and Goldstein, 2018).

Gene identification and phylogenetic analyses

Genes were identified as previously described (Heikes et al., 2023). Briefly, genes were identified in a published *Hypsibius exemplaris* transcriptome (Levin et al., 2016) by tBLASTn (Altschul et al., 1990; Gerts et al., 2006; Sayers et al., 2022) using protein sequences of known homologs in *Drosophila melanogaster* from the UCSC genome browser (Kent et al., 2002). A homolog for *fgf8* could not be found in this transcriptome but was identified in another (Yoshida et al., 2017). Top hits were confirmed by BLASTp (Sayers et al., 2022) against the *D. melanogaster* transcriptome and further confirmed through comparison of domains to the query sequence using SMART domain analysis tool in normal mode (Letunic et al., 2021; Letunic and Bork, 2018). Phylogenetic reconstructions were produced using alignments of conserved regions (either by manually-curated conserved domains or through the Gblocks program) (Castresana, 2000). Alignments were produced using Neighbor-Joining based MUSCLE alignment of curated protein sequences (Dereeper et al., 2008). Alignments were opened in Jalview to produce EPS files for figures. Alignments were also used to produce maximum likelihood phylogenetic reconstructions. Maximum phylogenetic reconstructions were produced comparing the top hits for each query to known homologs in various species in Mega-X (500 bootstraps), as previously described (Heikes et al., 2023; Kumar et al.,

2018). Accession numbers of protein sequences used in maximum likelihood reconstructions and species name abbreviations for all phylogenetic reconstructions are in Table 1.

Cloning

Genes were cloned as previously described (Heikes et al., 2023; Smith et al., 2016). Primers were designed using NCBI PrimerBLAST (Ye et al., 2012) to amplify genes by nested PCR. Primers are listed in Table 2.

Probe synthesis

RNA probes were synthesized as previously described (Heikes et al., 2023; Smith, 2018; Smith et al., 2016). Probes were labelled with either the DIG RNA labeling mix (Roche, Sigma product # 11277073910) or the Fluorescein RNA labeling mix (Roche, Sigma product # 11685619910) to facilitate double staining.

Fluorescence *in situ* hybridization

Fluorescence *in situ* hybridization (FISH) was performed using the Tyramide Signal Amplification kit from Akoya Biosciences, as previously described (Heikes et al., 2023), with the addition of a second round of antibody and signal amplification for double FISH. The added steps for double FISH performed were as follows, starting with the end of the tyramide signal amplification (steps 37-42) in the protocol previously published (Heikes et al., 2023). Embryos were washed in pre-heated Solution X for 20 minutes at 60°C (final concentrations: 50% formamide, 2x SSC, 1% SDS, diluted in DEPC-treated water) to inactivate peroxidase activity from the anti-DIG-POD antibody. Embryos were then washed four times quickly in 0.5x PBTw at room temperature. The protocol was then repeated starting from step 34 (Heikes et al., 2023) through to the end of the protocol, with the exception that anti-FITC-POD antibody was used to detect FITC-labelled RNA probes, instead of the anti-DIG-POD antibody used in the first round of detection. For both antibody incubations, a concentration of 1:500 antibody:blocking buffer was used. DIG-labelled probes were amplified with Cy3 amplification reagent (Akoya product # NEL744001KT) and FITC-labelled probes were amplified with Cy5 amplification reagent (Akoya product # NEL745001KT).

Fluorescence microscopy

FISH-stained embryos were imaged on a Zeiss LSM 710 microscope with a Plan-Neofluor 100x/1.3 oil Iris objective or a Zeiss LSM 880 microscopy with fast Airyscan detector and a Plan-Apochromat 63x/1.4 oil DIC objective. DAPI signal was excited with a 405 nm laser and collected between 411 and 543 nm. Cy3 signal was excited with a 560 nm laser and collected between 561 and 620 nm. Cy5 signal was excited with a 633 nm laser and collected between 639 and 750 nm. Images were opened in FIJI or Zen Black edition for image analysis. Minimum and Maximum displayed values were linearly adjusted in FIJI or Zen Black edition, and images were exported to scale in PNG format for cropping and annotation. Figures were made in Adobe Illustrator. Scale bars were added in Illustrator by pixel scale. DAPI stained DNA signal is displayed as blue in all figures. Cy3-amplified DIG-labelled probe signal is displayed in green in all figures, except for single-channel images, which are displayed in grayscale. Cy5-amplified FITC-labelled probe signal is displayed as magenta in all figures. Figure images are representative of detected patterns from at least ten embryos across at least two independent rounds of staining. Anterior is up in all images. Large dashed lines in figures indicate the boundary between the anterior and posterior of embryos.

Curating diagrams of development

Diagrams of development were hand-drawn on a Samsung Galaxy S8 tablet in the Concepts app, using fluorescent images to trace outlines and expression patterns.

Acknowledgements

We would like to express thanks to the many members of the Goldstein lab, past and present, for sharing in this research journey and promoting a supportive and creative lab environment conducive to research with an emerging model. In particular, we thank Frank Smith and members of the Smith lab for scientific discussions and for sharing unpublished results freely, and we also thank Lilly Papell for assistance with cloning the *doc1* and *eya Hypsibius exemplaris* homologs. We thank the UNC Biology Department, especially Tony Purdue and Nat Prunet for technical assistance in the UNC Biology microscopy core. We thank Dr. Amy Maddox, Dr. Amy Gladfelter, Dr. Greg Wray, and Dr. Christina Burch for helpful feedback on the manuscript and scientific discussions.

Funding

This work was supported by a grant from the National Science Foundation (IOS, 2028860 to BG), NIH Training Grant T32GM135128 to the UNC Curriculum in Genetics and Molecular Biology (KLH), and the UNC Chapel Hill Royster Society of Fellows (KLH).

Tables

Table 1 Accession numbers used for phylogenetic analysis

Accession Numbers for ML Protein Phylogenetic Reconstructions					
Species Abbrev.	**FGF8-like**	**Source**	**Sequence ID**	**Translation?**	**Species Name**
He	Fgf8	GenBank PRJNA360553	BV898_11515_t01	expasy	Hypsibius exemplaris
Dm	Ths	UCSC	NP_610701		Drosophila melanogaster
Ce	Egl-17	UCSC	NP_508107		Caenorhabditis elegans
Hv	FGF8	GenBank	XP_012554564.1		Hydra vulgaris
Sk	Fgf8	GenBank	ADB22412.1		Saccoglossus kowalevskii
Dr	Fgf8	GenBank	AAB82614.1		Danio rerio
Hs	Fgf8	GenBank	NP_149353.1		Homo sapiens
Bf	Fgf8	GenBank	XP_035674358.1		Branchiostoma floridae
Ci	Fgf8/17/18	GenBank	NP_001027648.1		Ciona intestinalis
Pf	Fgf8/17/18	GenBank	AKZ18202.1		Ptychodera flava
Nv	FGF8a	GenBank	ABN70836.1		Nematostella vectensis
Tt	Fgf8/17/18	GenBank	ALS19758.1		Terebratalia transversa
Na	Fgf8/17/18	GenBank	ALS19767.1		Novocrania anomala
Ph	Fgf8/17/18	GenBank	QUP08116.1		Phoronopsis harmeri
Species Abbrev.	**9/16/20 Family of FGFs**	**Source**	**Sequence ID**	**Translation?**	**Species Name**
Dm	Pyr	UCSC	NP_001097275		Drosophila melanogaster
Dm	Bnl	UCSC	NP_732452		Drosophila melanogaster
Ce	Let-756	UCSC	NP_498403		Caenorhabditis elegans

Nv	FGF9	GenBank	XP_032228973.1		Nematostella vectensis
Bf	FGF9	GenBank	XP_035675604.1		Branchiostoma floridae
Tt	FGF9/16/20	GenBank	QUP08106.1		Terebratalia transversa
Na	FGF9/16/20	GenBank	QUP08110.1		Novocrania anomala
Ph	FGF9/16/20	GenBank	QUP08115.1		Phoronopsis harmeri
Hv	FGF9	GenBank	AND74489.1		Hydra vulgaris
Ci	FGF9/16/20	GenBank	NP_001027649.1		Ciona intestinalis
Hs	FGF9	GenBank	NP_002001.1		Homo sapiens
Dr	FGF9	GenBank	XP_009302933.1		Danio rerio
Sk	FGF9	GenBank	NP_001161538		Saccoglossus kowalevskii
Species Abbrev.	**FGF Receptor-like**	**Source**	**Sequence ID**	**Translation?**	**Species Name**
He	FGFRL1	Levin et al., 2016 transcriptome	He_tr_04670	expasy	Hypsibius exemplaris
He	FGFRL2	Levin et al., 2016 transcriptome	He_tr_03639	expasy	Hypsibius exemplaris
Dm	Htl	UCSC	NP_732287		Drosophila melanogaster
Dm	Btl	UCSC	NP_729956		Drosophila melanogaster
Ce	Egl-15	UCSC	NP_001369987		Caenorhabditis elegans
Nv	FGFRa	GenBank	XP_048584433.1		Nematostella vectensis
Nv	FGFRb	GenBank	XP_048585038.1		Nematostella vectensis
Na	FGFR1	GenBank	QUP08111.1		Novocrania anomala
Tt	FGFR	GenBank	QUP08107.1		Terebratalia transversa
Ph	FGFR	GenBank	QUP08114.1		Phoronopsis harmeri
Hs	FGFR1	GenBank	AAH15035.1		Homo sapiens
Hs	FGFR2	GenBank	CAA96492.1		Homo sapiens

Hs	FGFR3	GenBank	XP_047305776.1		Homo sapiens
Hs	FGFR4	GenBank	NP_001341913.1		Homo sapiens
Bf	FGFR	GenBank	XP_035673320.1		Branchiostoma floridae
Species Abbrev.	**Non-FGFR RTKs**	**Source**	**Sequence ID**	**Translation?**	**Species Name**
He	VEGFR	Yanai	He_tr_02285	expasy	Hypsibius exemplaris
Dm	PVR	UCSC	NP_723365		Drosophila melanogaster
Ce	VER-1	UCSC	NP_497162		Caenorhabditis elegans
Ce	VER-3	UCSC	NP_509836		Caenorhabditis elegans
Ce	VER-4	UCSC	NP_509835		Caenorhabditis elegans
Hs	VGFR1	GenBank	NP_002010.2		Homo sapiens
Hs	VGFR2	GenBank	NP_002244.1		Homo sapiens
Hs	VGFR3	GenBank	NP_891555.2		Homo sapiens
Bf	VEGFR	GenBank	XP_035682136.1		Branchiostoma floridae
Species Abbrev.	**Snail**	**Source**	**Sequence ID**	**Translation?**	**Species Name**
He	Snail	Levin et al., 2016 transcriptome	Hduj_tr_05604	expasy	Hypsibius exemplaris
Dm	Snail	UCSC	NP_476732		Drosophila melanogaster
Dm	Escargot	UCSC	NP_476600		Drosophila melanogaster
Nv	SnaA	GenBank	AAR24456.1		Nematostella vectensis
Nv	SnaB	GenBank	AAR24457.1		Nematostella vectensis
Tc	Snail	GenBank	XP_971329.1		Tribolium castaneum
Hv	Snail	GenBank	XP_002162096.1		Hydra vulgaris
Ci	Snail	GenBank	AAB61226.1		Ciona intestinalis
Pf	Snail	GenBank	AXA20416.1		Ptychodera

					flava
Hs	SNAI1	GenBank	NP_005976.2		Homo sapiens
Bf	Snail	GenBank	AAC35351.1		Branchiostoma floridae
Species Abbrev.	**Scratch**	**Source**	**Sequence ID**	**Translation?**	**Species Name**
He	Scratch	Levin et al., 2016 transcriptome	Hduj_tr_06310	expasy	Hypsibius exemplaris
Dm	Scrt	UCSC	NP_523911.2		Drosophila melanogaster
Ce	CES-1	UCSC	NP_492338		Caenorhabditis elegans
Nv	Scratch2	GenBank	XP_032237161.1		Nematostella vectensis
Tc	Scratch1	GenBank	EFA13195.2		Tribolium castaneum
Tc	Scratch2	GenBank	EFA13196.1		Tribolium castaneum
Hs	Scratch1	GenBank	NP_112599.2		Homo sapiens
Hs	Scratch2	GenBank	NP_149120.1		Homo sapiens
Bf	Scratch1	GenBank	XP_035679385.1		Branchiostoma floridae
Bf	Scratch2	GenBank	XP_035679386.1		Branchiostoma floridae
Species Abbrev.	**Blimp-1**	**Source**	**Sequence ID**	**Translation?**	**Species Name**
He	Blimp-1	Levin et al., 2016 transcriptome	Hduj_tr_01892	expasy	Hypsibius exemplaris
Dm	Blimp-1	UCSC	NP_647982		Drosophila melanogaster
Bf	Blimp1	GenBank	ACH72078.1		Branchiostoma floridae
Species Abbrev.	**Dpp/BMP2/4**	**Source**	**Sequence ID**	**Translation?**	**Species Name**
He	Dpp	Levin et al., 2016 transcriptome	He_tr_08636	expasy	Hypsibius exemplaris
Dm	Dpp	UCSC	NP_477311		Drosophila melanogaster

Dm	Scw	UCSC	NP_524863		Drosophila melanogaster
Mm	BMP2	GenBank	NP_031579.2		Mus musculus
Mm	BMP4	GenBank	NP_001303289.1		Mus musculus
Nv	BMP2/4	GenBank	AAR13362.1		Nematostella vectensis
Tc	Dpp	GenBank	NP_001034540.1		Tribolium castaneum
Species Abbrev.	**Gbb/BMP5/7/8**	**Source**	**Sequence ID**	**Translation?**	**Species Name**
He	Gbb	Levin et al., 2016 transcriptome	He_tr_00999	expasy	Hypsibius exemplaris
Dm	Gbb	UCSC	NP_477340		Drosophila melanogaster
Mm	BMP5	GenBank	NP_031581.2		Mus musculus
Mm	BMP7	GenBank	NP_031583.2		Mus musculus
Mm	BMP8B	GenBank	NP_031585.2		Mus musculus
Mm	BMP8A	GenBank	NP_031584.1		Mus musculus
Nv	BMP5/7/8	GenBank	XP_032219054.1		Nematostella vectensis
Tc	Gbb	GenBank	NP_001107813.1		Tribolium castaneum
Species Abbrev.	**Other BMPs**	**Source**	**Sequence ID**	**Translation?**	**Species Name**
Mm	BMP3	GenBank	NP_775580.1		Mus musculus
Mm	BMP6	GenBank	NP_031582.1		Mus musculus
Mm	BMP9/GDF2	GenBank	NP_062379.3		Mus musculus
Mm	BMP10	GenBank	NP_033886.2		Mus musculus
Species Abbrev.	**Sog/Chordin**	**Source**	**Sequence ID**	**Translation?**	**Species Name**
He	sog	Levin et al., 2016 transcriptome	He_tr_06660	expasy	Hypsibius exemplaris
Dm	sog	UCSC	NP_001259578		Drosophila melanogaster
Mm	chordin	NCBI_GenBank	AAD19895.1		Mus musculus
Xl	chordin	NCBI_GenBank	AAC42222.1		Xenopus laevis

Tc	sog	NCBI_GenBank	ABF22614.1		Tribolium castaneum
Am	sog	NCBI_GenBank	XP_006570089.1		Apis mellifera
Hs	chordin	NCBI_GenBank	AAG35767.1		Homo sapiens
Ci	chordin	NCBI_GenBank	XP_026690585.1		Ciona intestinalis
Nv	chordin	NCBI_GenBank	ABC88373.1		Nematostella vectensis
Species Abbrev.	**Tkv/Type I receptor**	**Source**	**Sequence ID**	**Translation?**	**Species Name**
He	Tkv	Levin et al., 2016 transcriptome	He_tr_10719	expasy	Hypsibius exemplaris
Dm	Tkv	UCSC	NP_787989		Drosophila melanogaster
Gb	Tkv	NCBI_GenBank	AHJ59839.1		Gryllus bimaculatus
Tc	Tkv	NCBI_GenBank	EFA09250.1		Tribolium castaneum
Mm	BMPR1a	NCBI_GenBank	XP_036014306.1		Mus musculus
Nv	BMPR1b	NCBI_GenBank	XP_001633896.2		Nematostella vectensis
Species Abbrev.	**Punt/Type II receptor**	**Source**	**Sequence ID**	**Translation?**	**Species Name**
He	Punt	Levin et al., 2016 transcriptome	He_tr_12285	expasy	Hypsibius exemplaris
Dm	Punt	UCSC	NP_001262574		Drosophila melanogaster
Tc	Punt	NCBI_GenBank	EEZ97734.1		Tribolium castaneum
Mm	BMPR2	NCBI_GenBank	EDL00137.1		Mus musculus
Nv	BMPR2	NCBI_GenBank	XP_048588435.1		Nematostella vectensis
Species Abbrev.	**Sax/Type II receptor**	**Source**	**Sequence ID**	**Translation?**	**Species Name**
He	Sax	Levin et al., 2016 transcriptome	He_tr_01951	expasy	Hypsibius exemplaris
He	Babo	Levin et al., 2016 transcriptome	He_tr_12110	expasy	Hypsibius exemplaris

Dm	Sax	UCSC	NP_523652		Drosophila melanogaster
Dm	Babo	UCSC	NP_477000		Drosophila melanogaster
Tc	Babo	NCBI_GenBank	KYB28937.1		Tribolium castaneum
Tc	Sax	NCBI_GenBank	CDW20669.1		Tribolium castaneum
Dm	Wit	NP_524692	UCSC		Drosophila melanogaster
Tc	Wit	EFA07475.1	NCBI_GenBank		Tribolium castaneum
Species Abbrev.	**Tld**	**Source**	**Sequence ID**	**Translation?**	**Species Name**
He	Tld	Levin et al., 2016 transcriptome	Hduj_tr_05721	expasy	Hypsibius exemplaris
Dm	Tld	UCSC	NP_524487		Drosophila melanogaster
Dr	Tld	NCBI_GenBank	AAC60304.1		Danio rerio
Gg	Tld	NCBI_GenBank	NP_990034.2		Gallus gallus
Tc	Tld	NCBI_GenBank	KYB28517.1		Tribolium castaneum
Am	Tld	NCBI_GenBank	XP_006567026.2		Apis mellifera
Hs	Tld	NCBI_GenBank	KAI4027581.1		Homo sapiens
Ci	Tld	NCBI_GenBank	NP_001071840.1		Ciona intestinalis
Nv	Tld	NCBI_GenBank	XP_001633846.2		Nematostella vectensis
Species Abbrev.	**Doc1**	**Source**	**Sequence ID**	**Translation?**	**Species Name**
He	Doc1	Levin et al., 2016 transcriptome	HD_v1_tr_01406	expasy	Hypsibius exemplaris
Dm	Doc1	UCSC	NP_648283		Drosophila melanogaster
Tc	Doc	NCBI_GenBank	EFA10735.1		Tribolium castaneum
Mm	Tbx6	NCBI_GenBank	AAT72924.1		Mus musculus
Xl	Tbx6	NCBI_GenBank	ABC75836.1		Xenopus laevis
Xl	VegT	NCBI_GenBank	AAB93301.1		Xenopus laevis

Mm	Brachyury	NCBI_GenBank	AAI20808.1		Mus musculus
Mm	Tbx2	NCBI_GenBank	AAC52697.1		Mus musculus
Mm	Tbx20	NCBI_GenBank	NP_919239.1		Mus musculus
He	Omb	Levin et al., 2016 transcriptome	Hduj_tr_06618	expasy	Hypsibius exemplaris
Dm	Omb	UCSC	NP_525070		Drosophila melanogaster
Species Abbrev.	**Eya**	**Source**	**Sequence ID**	**Translation?**	**Species Name**
He	Eya	Levin et al., 2016 transcriptome	HD_v1_tr_10204	expasy	Hypsibius exemplaris
Dm	Eya	UCSC	NP_723188		Drosophila melanogaster
Ce	Eya-1	UCSC	NP_001367120		Caenorhabditis elegans
Mm	Eya1	NCBI_GenBank	NP_001297388.1		Mus musculus
Dr	Eya1	NCBI_GenBank	AAI54188.1		Danio rerio
Hs	Eya1	NCBI_GenBank	AAI21799.1		Homo sapiens
Nv	Eya	NCBI_GenBank	XP_032233587.1		Nematostella vectensis
At	Eya	NCBI_GenBank	NP_565803.1		Arabidopsis thaliana

Table 2 Primers used for cloning

Primers		
Target	**Direction**	**Sequence (5' → 3')**
dpp	F1	acctgacgagcgtacattcc
	R1	aactgctccagccaatctcc
	F2	ccgcttctaacggctcatcc
	R2	ccccggcgatacttcttcac
gbb	F1	acggcatcgaccaatccatc
	R1	gtaggccgagtaaccatccg
	F2	atcgaccaatccatcccgc
	R2	gaagaacgccaccatgaagc
sog	F1	agcagcagcagtatcgtttg
	R1	tccgtcgagaatccttagcc
	F2	cagcagcagtatcgtttgtttg
	R2	taatggtccccttgtagccg
tkv	F1	tccttcatcttttgcgtggc
	R1	ctctggggtggtagtcagtg
	F2	aacagtaaatgcttcgccgc
	R2	ccaagaaggttgtcgtgtcg
punt	F1	ctatggggaggtgtggaagg
	R1	catgcgattgagcagacagg
	F2	tatggggaggtgtggaaggg
	R2	agggtttgaaggaaggtcgg
fgf8	F1	taatcgtcttccttgcagcc
	R1	tagaggagggtcttcagcg
	F2	gcagcctcatcccttcttc
	R2	ccggtggaagttgtagcag
fgfrl1	F1	agcggaatttacaactgcac
	R1	aactttgggtgttttgacgg
	F2	atatcatggggtcgcatcc
	R2	caatggttcgttcctccttg

fgfrl2	F1	acggactctcacaatcagac
	R1	caagagcagcaacatgactc
	F2	catccttcatccaactgggg
	R2	ggcaatgtttttctgcattcg
snail	F1	cctcccatactttccgtctc
	R1	tcaggcatatcaggcacttg
	F2	caacaacttctcaccgttcc
	R2	agattttgcagtcgtaaggc
tld	F1	agacccttcttatgcccaac
	R1	atacagctctggaaaggacg
	F2	agcaaagagtgccagttagg
	R2	aaagatggtcccgttcaagg
doc1	F1	gatacactccagtctcctgc
	R1	tgaacaaaacgggaacatgg
	F2	tctcctgccaatcatgtacc
	R2	aaggtctcggaagcctttag
eya	F1	acaatatggagcgcgttttc
	R1	caggtgatcattctccaggg
	F2	atagacccacattcgacacg
	R2	ctgcaggttaagcagttgtg

Table 3 Testable Hypotheses of FGF and BMP Functions

Pathway(s)	Relevant Pattern	Hypothesis
FGF	*fgf8* patches form dynamically over time	A gene such as Ets4 induces patch formation
	fgf8 patches increase in number and decrease in size	Patches arise from independent cell populations
	fgf8 patches change orientation relative to embryo axes	The same cells expressing fgf8 tangential to the A-P axis then move to be perpendicular to the A-P axis
	fgf8 patches occur adjacent to the ectodermal furrow sites	patches regulate ectodermal furrow formation
	fgf8 patches occur in layer above endomesodermal pouches	FGF8 guides migration of underlying mesoderm
	fgf8 patches occur in layer above endomesodermal pouches	FGF8 patterns muscle-body wall attachment sites
	fgf8 patches occur in layer above endomesodermal pouches	FGF8 regulates fate commitment of mesodermal cells
	fgf8 patches occur in the posterior of body segments	FGF8 provides posterior cues along the A-P axis of body segments
	fgf8 patches occur in layer above endomesodermal pouches; *eya* is enriched in endomesoderm	FGF8 regulates *eya* expression
BMP	*dpp* extends more dorsally than *sog* laterally along the embryo	Dpp regulates D-V patterning
	dpp extends more dorsally than *sog* laterally along the embryo	Dpp informs D-V position of future limbs
	dpp extends more dorsally than *sog* laterally along the embryo	Sog prevents limbs from forming too far ventrally or in internal cells
	dpp extends more dorsally than *sog* laterally along the embryo	Dpp regulates cuticle deposition and patterning
	sog bands on either side of developing mouth; *dpp* beyond and overlapping *sog* bands	Dpp inhibits mouth formation and Sog limits the inhibitory function of Dpp
	dpp is expressed in ectoderm above endomesoderm	Dpp regulates mesoderm development
	gbb is enriched in most cells except PGCs; *tkv* and *punt* are enriched in most cells including the PGCs	Gbb regulates PGC fate acquisition, maintenance, and/or development
	sog bands on either side of developing mouth; *dpp* beyond and overlapping *sog* bands; *tld* stretches between *sog* bands	Tld facilitates spreading of Dpp (with Sog) to the developing mouth or to the anterior endomesodermal pouches
	tld expressed across developing mouth	Tld regulates pharyngeal development

		through control of ECM independent of Dpp
	snail expressed in ectoderm and endomesoderm	non-mesodermal cells express snail early and later snail expression is restricted to mesoderm
	doc1 enriched in dorsal stripe; *dpp* extends more dorsally than *sog* laterally along the embryo	Dpp regulates *doc1* expression
	dpp is expressed in ectoderm above endomesoderm; *eya* enriched in endomesoderm	Dpp regulates *eya* expression
	gbb is enriched in most cells except PGCs; *tkv* and *punt* are enriched in most cells including the PGCs; *eya* is expressed in PGCs	Gbb regulates *eya* expression in PGCs and/or the entire embryo
BMP+FGF	*fgf8* and *dpp* enriched in ectoderm	Fgf8 and Dpp work together to regulate proper mesoderm formation and/or fate specification

References

Aguinaldo, A.M.A., Turbevillet, J.M., Linford, L.S., Rivera, M.C., Garey:T:, J.R., Raff, R.A., Lake, J.A., 1997. Evidence for a clade of nematodes, arthropods and other moulting animals. Nature 387, 489–493. https://doi.org/https://doi.org/10.1038/387489a0

Ahrens, K., Schlosser, G., 2005. Tissues and signals involved in the induction of placodal Six1 expression in Xenopus laevis 288, 40–59. https://doi.org/10.1016/j.ydbio.2005.07.022

Akiyama-Oda, Y., Oda, H., 2006. Axis specification in the spider embryo: Dpp is required for radial-to-axial symmetry transformation and sog for ventral patterning. Development 133, 2347–2357. https://doi.org/10.1242/dev.02400

Akiyama-Oda, Y., Oda, H., 2003. Early patterning of the spider embryo: A cluster of mesenchymal cells at the cumulus produces Dpp signals received by germ disc epithelial cells. Development 130, 1735–1747. https://doi.org/10.1242/dev.00390

Alberga, A., Boulay, J., Kempe, E., Dennefeld, C., Haenlin, M., 1991. The snail gene required for mesoderm formation in Drosophila is expressed dynamically in derivatives of all three germ layers. Development 111, 983–992. https://doi.org/doi.org/10.1242/dev.111.4.983

Altschul, S.F., Gish, W., Miller, W., Myers, E.W., Lipman, D.J., 1990. Basic local alignment search tool. J. Mol. Biol. 215, 403–410. https://doi.org/10.1016/S0022-2836(05)80360-2

Andrikou, C., Hejnol, A., 2021. FGF signaling acts on different levels of mesoderm development within Spiralia. Dev. 148. https://doi.org/10.1242/DEV.196089

Arendt, D., Nubler-Jung, K., 1994. Inversion of dorsoventral axis ? Nature 371, 26.

Ashe, H.L., Levine, M., 1999. Local inhibition and long-range enhancement of Dpp signal transduction by Sog. Nature 398, 427–431. https://doi.org/10.1038/18892

Birnbaum, D., Popovici, C., Roubin, R., 2005. A pair as a minimum: The two fibroblast growth factors of the nematode Caenorhabditis elegans. Dev. Dyn. 232, 247–255. https://doi.org/10.1002/dvdy.20219

Cano, A., Pérez-moreno, M.A., Rodrigo, I., Locascio, A., Blanco, M.J., Barrio, M.G., Portillo, F., Nieto, M.A., 2000. The transcription factor Snail controls epithelial – mesenchymal transitions by repressing E-cadherin expression 2.

Castresana, J., 2000. Selection of conserved blocks from multiple alignments for their use in phylogenetic analysis. Mol. Biol. Evol. 17, 540–552. https://doi.org/10.1093/oxfordjournals.molbev.a026334

Chavarria, R.A., Game, M., Arbelaez, B., Ramnarine, C., Snow, Z.K., Smith, F.W., 2021. Extensive loss of Wnt genes in Tardigrada. BMC Ecol. Evol. 21, 1–21.

https://doi.org/10.1186/s12862-021-01954-y

Chopra, V.S., Levine, M., 2009. Combinatorial patterning mechanisms in the Drosophila embryo 8. https://doi.org/10.1093/bfgp/elp026

Dale, L., Howes, G., Price, B.M.J., Smith, J.C., 1992. Bone morphogenetic protein 4: A ventralizing factor in early Xenopus development. Development 115, 573–585. https://doi.org/10.1242/dev.115.2.573

Dereeper, A., Guignon, V., Blanc, G., Audic, S., Buffet, S., Chevenet, F., Dufayard, J.F., Guindon, S., Lefort, V., Lescot, M., Claverie, J.M., Gascuel, O., 2008. Phylogeny.fr: robust phylogenetic analysis for the non-specialist. Nucleic Acids Res. 36, 465–469. https://doi.org/10.1093/nar/gkn180

Dominguez, C., Zuñiga, A., Hanna, P., Hodar, C., Gonzalez, M., Cambiazo, V., 2016. Target genes of Dpp/BMP signaling pathway revealed by transcriptome profiling in the early D. melanogaster embryo. Gene 592, 191–200. https://doi.org/10.1016/j.gene.2016.07.015

Donoughe, S., Nakamura, T., Ewen-Campen, B., Green, D.A., Henderson, L., Extavour, C.G., 2014. BMP signaling is required for the generation of primordial germ cells in an insect. Proc. Natl. Acad. Sci. U. S. A. 111, 4133–4138. https://doi.org/10.1073/pnas.1400525111

Ferguson, E.L., Anderson, K. V., 1992. decapentaplegic acts as a morphogen to organize dorsal-ventral pattern in the Drosophila embryo. Cell 71, 451–461. https://doi.org/10.1016/0092-8674(92)90514-D

François, V., Solloway, M., O'Neill, J.W., Emery, J., Bier, E., 1994. Dorsal-ventral patterning of the Drosophila embryo depends on a putative negative growth factor encoded by the short gastrulation gene. Genes Dev. 8, 2602–2616. https://doi.org/10.1101/gad.8.21.2602

Frasch, M., 1995. Induction of visceral and cardiac mesoderm by ectodermal dpp in the early drosophila embryo. Nature 374, 464–467. https://doi.org/10.1038/374464a0

Gabriel, W.N., Goldstein, B., 2007. Segmental expression of Pax3 / 7 and Engrailed homologs in tardigrade development. Dev. Genes Evol. 217, 421–433. https://doi.org/10.1007/s00427-007-0152-5

Gabriel, W.N., Mcnuff, R., Patel, S.K., Gregory, T.R., Jeck, W.R., Jones, C.D., Goldstein, B., 2007. The tardigrade Hypsibius dujardini, a new model for studying the evolution of development. Dev. Biol. 312, 545–559. https://doi.org/10.1016/j.ydbio.2007.09.055

Game, M., Smith, F.W., 2020. Loss of intermediate regions of perpendicular body axes contributed to miniaturization of tardigrades. Proc. R. Soc. B Biol. Sci. 287. https://doi.org/10.1098/rspb.2020.1135

Gerts, E.M., Yu, Y.K., Agarwala, R., Schäffer, A.A., Altschul, S.F., 2006. Composition-based statistics and translated nucleotide searches: Improving the TBLASTN module of BLAST. BMC Biol. 4, 1–14. https://doi.org/10.1186/1741-7007-4-41

Goldstein, B., 2022a. Tardigrades and their emergence as model organisms, 1st ed, Current Topics in Developmental Biology. Elsevier Inc. https://doi.org/10.1016/bs.ctdb.2021.12.008

Goldstein, B., 2022b. Tardigrades, Creature Column. Nat. Methods 19, 903. https://doi.org/10.1038/s41592-022-01564-6

Goldstein, B., 2018. The Emergence of the Tardigrade Hypsibius exemplaris as a Model System. Cold Spring Harb. Protoc. 859–866. https://doi.org/10.1101/pdb.emo102301

Goldstein, B., Blaxter, M., 2002. Quick guide Tardigrades. Curr. Biol. 12, 475.

Goto, S., Hayashi, S., 1997. Specification of the embryonic limb primordium by graded activity of Decapentaplegic. Development 124, 125–132. https://doi.org/10.1242/dev.124.1.125

Heikes, K.L., Game, M., Smith, F.W., Goldstein, B., 2023. The Embryonic Origin of Primordial Germ Cells in the Tardigrade Hypsibius exemplaris. Dev. Biol. 497, 42–58. https://doi.org/10.1016/j.ydbio.2023.02.008

Heikes, K.L., Goldstein, B., 2018. Live imaging of tardigrade embryonic development by differential interference contrast microscopy. Cold Spring Harb. Protoc. 874–877. https://doi.org/10.1101/pdb.prot102335

Holley, S.A., Jacksont, P.D., Sasalt, Y., Lut, B., Robertlst, E.M. De, Hoffmannt, F.M., Ferguson, E.L., 1995. A conserved system for dorsal-ventral patterning in insects and vertebrates involving sog and chordin 376, 249–253.

Huang, P., Stern, M.J., 2005. FGF signaling in flies and worms: More and more relevant to vertebrate biology. Cytokine Growth Factor Rev. 16, 151–158. https://doi.org/10.1016/j.cytogfr.2005.03.002

Jones, C.M., Lyons, K.M., Lapan, P.M., Wright, C.V.E., Hogan, B.L.M., 1992. DVR-4 (Bone Morphogenetic Protein-4) as a posterior-ventralizing factor in Xenopus mesoderm induction. Development 115, 639–647. https://doi.org/10.1242/dev.115.2.639

Kawakami, Y., Capdevila, J., Büscher, D., Itoh, T., Esteban, C.R., Belmonte, J.C.I., 2001. WNT signals control FGF-dependent limb initiation and AER induction in the chick embryo. Cell 104, 891–900. https://doi.org/10.1016/S0092-8674(01)00285-9

Kent, W.J., Sugnet, C.W., Furey, T.S., Roskin, K.M., Pringle, T.H., Zahler, A.M., Haussler, and D., 2002. The Human Genome Browser at UCSC. Genome Res. 12, 996–1006. https://doi.org/10.1101/gr.229102

Kondo, K., Tanaka, A., Kunieda, T., 2024. Single-step generation of homozygous knock-out/knock-in individuals in an extremotolerant parthenogenetic tardigrade using DIPA-CRISPR. bioRxiv Prepr. https://doi.org/doi.org/10.1101/2024.01.10.575120

Kumagai, H., Kondo, K., Kunieda, T., 2022. Application of CRISPR/Cas9 system and

the preferred no-indel end-joining repair in tardigrades. Biochem. Biophys. Res. Commun. 623, 196–201. https://doi.org/10.1016/j.bbrc.2022.07.060

Kumar, S., Stecher, G., Li, M., Knyaz, C., Tamura, K., 2018. MEGA X: Molecular evolutionary genetics analysis across computing platforms. Mol. Biol. Evol. 35, 1547–1549. https://doi.org/10.1093/molbev/msy096

Lawson, K.A., Dunn, N.R., Roelen, B.A.J., Zeinstra, L.M., Davis, A.M., Wright, C.V.E., Korving, J.P.W.F.M., Hogan, B.L.M., 1999. Bmp4 is required for the generation of primordial germ cells in the mouse embryo 424–436.

Leptin, M., 1991. twist and snail as positive and negative regulators during Drosophila mesoderm development. Genes Dev. 5, 1568–1576. https://doi.org/10.1101/gad.5.9.1568

Letunic, I., Bork, P., 2018. 20 years of the SMART protein domain annotation resource. Nucleic Acids Res. 46, D493–D496. https://doi.org/10.1093/nar/gkx922

Letunic, I., Khedkar, S., Bork, P., 2021. SMART: Recent updates, new developments and status in 2020. Nucleic Acids Res. 49, D458–D460. https://doi.org/10.1093/nar/gkaa937

Levin, M., Anavy, L., Cole, A.G., Winter, E., Mostov, N., Khair, S., Senderovich, N., Kovalev, E., Silver, D.H., Feder, M., Fernandez-Valverde, S.L., Nakanishi, N., Simmons, D., Simakov, O., Larsson, T., Liu, S.-Y., Jerafi-Vider, A., Yaniv, K., Ryan, J.F., Martindale, M.Q., Rink, J.C., Arendt, D., Degnan, S.M., Degnan, B.M., Hashimshony, T., Yanai, I., 2016. The mid-developmental transition and the evolution of animal body plans. Nature 531, 637–641. https://doi.org/10.1038/nature16994

Lo, T.W., Bennett, D.C., Goodman, S.J., Stern, M.J., 2010. Caenorhabditis elegans fibroblast growth factor receptor signaling can occur independently of the multi-substrate adaptor FRS2. Genetics 185, 537–547. https://doi.org/10.1534/genetics.109.113373

Lochab, A.K., Extavour, C.G., 2017. Bone Morphogenetic Protein (BMP) signaling in animal reproductive system development and function. Dev. Biol. 427, 258–269. https://doi.org/10.1016/j.ydbio.2017.03.002

Luo, K., 2017. Signaling Cross Talk between TGF-b / Smad and Other Signaling Pathways. Cold Spring Harb. Persepctives Biol. 9, 1–28.

Marcus, E., 1929. Zur Embryologie der Tardigraden. Zool. Jahrbücher, Abteilung für Anat. und Ontog. der Tiere 50, 333–384. https://doi.org/10.23736/S0392-9590.16.03730-5

Martinez, P., 2018. The Comparative Method in Biology and the Essentialist Trap 6, 1–5. https://doi.org/10.3389/fevo.2018.00130

Matus, D.Q., Thomsen, G.H., Martindale, M.Q., 2007. FGF signaling in gastrulation and neural development in Nematostella vectensis, an anthozoan cnidarian. Dev. Genes Evol. 217, 137–148. https://doi.org/10.1007/s00427-006-0122-3

Mcnuff, R., 2018. Laboratory Culture of Hypsibius exemplaris. Cold Spring Harb. Protoc. 867–870. https://doi.org/10.1101/pdb.prot102319

Morisato, D., Anderson, K. V., 1995. Signaling pathways that establish the dorsal-ventral pattern of the Drosophila embryo. Annu. Rev. Genet. 29, 371–399. https://doi.org/10.1146/annurev.genet.29.1.371

Muha, V., Müller, H.A.J., 2013. Functions and mechanisms of fibroblast growth factor (FGF) signalling in Drosophila melanogaster. Int. J. Mol. Sci. 14, 5920–5937. https://doi.org/10.3390/ijms14035920

Mullins, M.C., 1998. Holy Tolloido: Tolloid cleaves SOG/Chordin to free DPP/BMPs. Trends Genet. 14, 127–129. https://doi.org/10.1016/S0168-9525(98)01431-0

Nakayama, T., Cui, Y., Christian, J.L., 2000. Regulation of BMP / Dpp signaling during embryonic development 57, 943–956.

Nunes da Fonseca, R., van der Zee, M., Roth, S., 2010. Evolution of extracellular Dpp modulators in insects: The roles of tolloid and twisted-gastrulation in dorsoventral patterning of the Tribolium embryo. Dev. Biol. 345, 80–93. https://doi.org/10.1016/j.ydbio.2010.05.019

Pires-daSilva, A., Sommer, R.J., 2003. THE EVOLUTION OF SIGNALLING PATHWAYS IN ANIMAL DEVELOPMENT. Nat. Rev. Genet. 4, 39–49. https://doi.org/10.1038/nrg977

Ramel, M.C., Hill, C.S., 2012. Spatial regulation of BMP activity. FEBS Lett. 586, 1929–1941. https://doi.org/10.1016/j.febslet.2012.02.035

Rasmussen, J.P., Reddy, S.S., Priess, J.R., 2012. Laminin is required to orient epithelial polarity in the C. elegans pharynx. Development 139, 2050–2060. https://doi.org/10.1242/dev.078360

Rentzsch, F., Fritzenwanker, J.H., Scholz, C.B., Technau, U., 2008. FGF signalling controls formation of the apical sensory organ in the cnidarian Nematostella vectensis. Development 135, 1761–1769. https://doi.org/10.1242/dev.020784

Row, R.H., Pegg, A., Kinney, B.A., Farr, G.H., Maves, L., Lowell, S., Wilson, V., Martin, B.L., 2018. BMP and FGF signaling interact to pattern mesoderm by controlling basic helix-loop-helix transcription factor activity 1–27.

Sasai, Y., Lu, B., Steinbeisser, H., Geissert, D., Gont, L.K., Robertis, E.M. De, 1994. Xenopus chordin : A Novel Dorsalizing Factor Activated by Organizer-Specific Homeobox Genes 79, 779–790.

Sayers, E.W., Bolton, E.E., Brister, J.R., Canese, K., Chan, J., Comeau, D.C., Connor, R., Funk, K., Kelly, C., Kim, S., Madej, T., Marchler-Bauer, A., Lanczycki, C., Lathrop, S., Lu, Z., Thibaud-Nissen, F., Murphy, T., Phan, L., Skripchenko, Y., Tse, T., Wang, J., Williams, R., Trawick, B.W., Pruitt, K.D., Sherry, S.T., 2022. Database resources of the national center for biotechnology information. Nucleic Acids Res. 50, D20–D26. https://doi.org/10.1093/nar/gkab1112

Schill, R.O., 2018. Water Bears: The Biology of Tardigrades. Springer. https://doi.org/10.1007/978-3-319-95702-9

Sharma, R., Beer, K., Iwanov, K., Schmöhl, F., Beckmann, P.I., Schröder, R., 2015. The single fgf receptor gene in the beetle Tribolium castaneum codes for two isoforms that integrate FGF8-and Branchless-dependent signals. Dev. Biol. 402, 264–275. https://doi.org/10.1016/j.ydbio.2015.04.001

Sharma, R., Beermann, A., Schröder, R., 2013. FGF signalling controls anterior extraembryonic and embryonic fate in the beetle Tribolium. Dev. Biol. 381, 121–133. https://doi.org/10.1016/j.ydbio.2013.05.031

Shimmi, O., O'Connor, M.B., 2003. Physical properties of Tld, Sog, Tsg and Dpp protein interactions are predicted to help create a sharp boundary in Bmp signals during dorsoventral patterning of the Drosophila embryo. Development 130, 4673–4682. https://doi.org/10.1242/dev.00684

Shimmi, O., Umulis, D., Othmer, H., Connor, M.B.O., 2005. Facilitated Transport of a Dpp / Scw Heterodimer by Sog / Tsg Leads to Robust Patterning of the Drosophila Blastoderm Embryo 120, 873–886. https://doi.org/10.1016/j.cell.2005.02.009

Simpson, P., 1983. Maternal-zygotic gene interactions during formation o f t h e dorsoventral pattern in drosophila embryos. Genetics 105, 615–632. https://doi.org/doi.org/10.1093/genetics/105.3.615

Smith, F.W., 2018. Embryonic In Situ Hybridization for the Tardigrade Hypsibius exemplaris. Cold Spring Harb. Protoc. 891–899. https://doi.org/10.1101/pdb.prot102350

Smith, F.W., Boothby, T.C., Giovannini, I., Rebecchi, L., Jockusch, E.L., Goldstein, B., 2016. The Compact Body Plan of Tardigrades Evolved by the Loss of a Large Body Region. Curr. Biol. 26, 224–229. https://doi.org/10.1016/j.cub.2015.11.059

Smith, F.W., Cumming, M., Goldstein, B., 2018. Analyses of nervous system patterning genes in the tardigrade Hypsibius exemplaris illuminate the evolution of panarthropod brains. Evodevo 9, 1–23. https://doi.org/10.1186/s13227-018-0106-1

Smith, F.W., Game, M., Mapalo, M.A., Chavarria, R.A., Harrison, T.R., Janssen, R., 2023. Developmental and genomic insight into the origin of the tardigrade body plan. Evol. Dev. 1–18. https://doi.org/10.1111/ede.12457

Spencer, F.A., Hoffmann, F.M., Gelbart, W.M., 1982. Decapentaplegic: A gene complex affecting morphogenesis in Drosophila melanogaster. Cell 28, 451–461. https://doi.org/10.1016/0092-8674(82)90199-4

Staehllng-hampton, K., Hoffmann, F.M., Bayliest, M.K., Rushtont, E., Batett, M., 1994. dpp induces mesodermal gene expression in Drosophila 372, 783–786.

Stathopoulos, A., Tam, B., Ronshaugen, M., Frasch, M., Levine, M., 2004. Pyramus and thisbe: FGF genes that pattern the mesoderm of Drosophila embryos. Genes Dev. 18, 687–699. https://doi.org/10.1101/gad.1166404

Tanaka, S., Aoki, K., Arakawa, K., 2022. in vivo expression vector derived from anhydrobiotic tardigrade genome enables live imaging in Eutardigrada. bioRxiv Prepr. https://doi.org/doi.org/10.1101/2022.09.21.508853

Tu, Q., Cameron, R.A., Davidson, E.H., 2014. Quantitative developmental transcriptomes of the sea urchin Strongylocentrotus purpuratus. Dev. Biol. 385, 160–167. https://doi.org/10.1016/j.ydbio.2013.11.019

Vadon-Le Goff, S., Hulmes, D.J.S., Moali, C., 2015. BMP-1/tolloid-like proteinases synchronize matrix assembly with growth factor activation to promote morphogenesis and tissue remodeling. Matrix Biol. 44–46, 14–23. https://doi.org/10.1016/j.matbio.2015.02.006

Van Der Zee, M., Stockhammer, O., Von Levetsow, C., Nunes Da Fonseca, R., Roth, S., 2006. Sog/chordin is required for ventral-to-dorsal Dpp/BMP transport and head formation in a short germ insect. Proc. Natl. Acad. Sci. U. S. A. 103, 16307–16312. https://doi.org/10.1073/pnas.0605154103

Wang, R., Leite, D.J., Karadas, L., Schiffer, P.H., Pechmann, M., 2023. FGF signalling is involved in cumulus migration in the common house spider Parasteatoda tepidariorum. Dev. Biol. 494, 35–45. https://doi.org/10.1016/j.ydbio.2022.11.009

Wharton, K.A., Ray, R.P., Gelbart, W.M., 1993. An activity gradient of decapentaplegic is necessary for the specification of dorsal pattern elements in the Drosophila embryo. Development 117, 807–822. https://doi.org/10.1242/dev.117.2.807

Winnier, G., Blessing, M., Labosky, P.A., Brigid, L.M.H., 1995. Bone morphogenetic protein-4 is required for mesoderm formation and patterning in the mouse. Genes Dev. 9, 2105–2116.

Winstanley, J., Sawala, A., Baldock, C., Ashe, H.L., 2015. Synthetic enzyme-substrate tethering obviates the Tolloid-ECM interaction during Drosophila BMP gradient formation. Elife 4, 1–18. https://doi.org/10.7554/eLife.05508

Ye, J., Coulouris, G., Zaretskaya, I., Cutcutache, I., Rozen, S., Madden, T.L., 2012. Primer-BLAST: A tool to design target-specific primers for polymerase chain reaction Jian. BMC Bioinformatics 13.

Yoshida, Y., Koutsovoulos, G., Laetsch, D.R., Stevens, L., Kumar, S., Horikawa, D.D., Ishino, K., Komine, S., Kunieda, T., Tomita, M., Blaxter, M., Arakawa, K., 2017. Comparative genomics of the tardigrades Hypsibius dujardini and Ramazzottius varieornatus, PLoS Biology. https://doi.org/10.1371/journal.pbio.2002266

Figure Legends

Figure 1 Introduction to morphology of *Hypsibius exemplaris* embryos between elongation and segmentation stages.

A. Drawings representative of *H. exemplaris* embryos at elongation, endomesodermal pouch formation (E.P.), and ectodermal segmentation (E.S.) stages, shown from right lateral and ventral views. From top to bottom, images show surface to internal views (and dorsal surface for ventral views). Anterior (A) is up and Posterior (P) is down in all drawings. Dorsal (D) and (V) are to the left and right, respectively, in the lateral views. Certain morphological features are labelled: mouth (mo), anterior mesoderm (am), dorsal midline (dm), foregut (fg), endomesoderm (em), endomesodermal pouch (ep), trunk segment (t), and primordial germ cells (pgcs). B. Schematic of FGF signaling showing extracellular ligand (green) binding transmembrane receptors (magenta), which dimerize. C. Schematic of BMP signaling showing extracellular ligand (green) binding extracellular antagonist (magenta), which is cleaved by extracellular protease (orange), free the ligand to bind transmembrane receptors (blue), which form a heterotetramer.

Figure 2 Expression patterns of *fgf8* and *fgfrl1* mRNAs at 24 hpl reveal ectodermal patches of *fgf8* in segment posteriors and endomesodermal enrichment of *fgfrl1*.

A-D. Expression patterns of *fgf8* and *fgfrl1* at 24 hpl. A-B. Maximum intensity projections of embryos from a dorsolateral (A) and lateral (B) view. C. Projection of uppermost layers of the embryo in B. D. Projection of internal layers of the embryo in B. Small region outlined with a dashed line indicates the upper layers projected in C, which are omitted in the internal layers projected in D. Arrowheads indicate ectodermal patches of *fgf8* signal in trunk segment posteriors. Blue arrowheads indicate two of the ectodermal patches of *fgf8* signal running along the left side of the embryo in A. Orange arrowheads indicate the anterior head segment patch of *fgf8* signal. Arrows indicate small groups of ectodermal and endomesodermal cells enriched for *fgf8* at the posterior of head segments. Right dorsolateral view in A. Left lateral view in B-D. Scale bar = 10 μm.

Figure 3 Lateral ectoderm patches of *fgf8* mRNA arise prior to ectodermal segmentation and near the time of endomesodermal pouch formation.

A-D. Expression patterns of *fgf8* and *fgfrl1* mRNAs at 19 hpl (A) 20 hpl (B) 21 hpl (C) and 22 hpl (D). All images are maximum intensity projections of embryo from lateral views. Arrowheads indicate ectodermal patches of *fgf8* signal. Orange arrowheads indicate the patch of *fgf8* signal in the anterior of head segments. Arrows indicate small groups of cells enriched for *fgf8* at the posterior of head segments. Left lateral view in A-C. Right lateral view in D. Scale bar = 10 μm.

Figure 4 mRNA of the mesodermal transcription factor *snail* is present in non-mesodermal cells.

A-B. Enrichment patterns of *snail* and *fgfrl1* mRNAs at 18 hpl (A) and 24 hpl (B). C-D. Enrichment patterns of *snail* and *fgf8* mRNAs at 19 hpl (A) and 24 hpl (B). All images are maximum intensity projections. Arrowheads indicate ectodermal patches of *fgf8* signal. Orange arrowheads indicate the patch of *fgf8* signal in the anterior of head segments. Arrows indicate small groups of cells enriched for *fgf8* at the posterior of head segments. Right lateral view in A-C. Right ventrolateral view in D. Scale bar = 10 μm.

Figure 5 mRNAs of BMP ligand *dpp* and antagonist *sog* are expressed in lateral ectoderm, with *dpp* expressed more dorsally than *sog.*

A-D. Enrichment patterns of *dpp* and *sog* mRNAs at 24 hpl. A and C Maximum intensity projections of embryos from a dorsal (A) and lateral (C) view. B. Projection of internal layers of the embryo in A. D. Projection of internal layers of the embryo in C. Arrowheads indicate the extent of spread of *dpp* mRNA dorsally. Orange arrowheads indicate the absence of enrichment for *dpp* and *sog* at the dorsal midline of the embryo. Arrows in A-B indicate bands of cells enriched for *sog* on either side of the developing mouth. Arrows in C-D indicate the endomesodermal cells enriched for *sog* in each endomesodermal pouch. Asterisks in A-B indicate the hollow space within the developing foregut, which is not enriched for *sog* in its epithelium. Dorsal view in A and B. Right lateral view in C and D. Scale bar = 10 μm.

Figure 6 Expression of *dpp* and *sog* mRNAs changes between elongation and segmentation.

A-C. Enrichment patterns of *dpp* and *sog* mRNAs at 18 hpl (A) 19 hpl (B) and 20 hpl (C). All images are maximum intensity projections. Arrowheads indicate the extent *dpp* mRNA expression dorsally. Orange arrowheads indicate the absence of enrichment for *dpp* and *sog* at the dorsal midline. Arrows indicate bands of cells enriched for *sog* on either side of the developing mouth. Blue arrowheads indicate bands of *dpp* running over each segment. Left ventrolateral view in A. Dorsal view in B. Right ventrolateral view in C. Left dorsolateral view in D. Scale bar = 10 μm.

Figure 7 mRNAs of protease tld become more restricted along the anterior-most ridge of the head from 19 to 24 hpl.

A-C. Enrichment patterns of *tld* and *sog* mRNAs at 19 hpl (A), 20 hpl (B), and 24 hpl (C). D Enrichment patterns of *tld* and *dpp* mRNAs at 24 hpl. All images are maximum intensity projections. Arrowheads indicate the band of *tld* along the anterior ridge of the embryo. Arrows indicate bands of cells enriched for *sog* on either side of the developing mouth. Orange arrowheads indicate the bands of *dpp* running over each segment. Dorsal view in A. Left ventrolateral view in B-C. Left lateral view in D. Scale bar = 10 μm.

Figure 8 Expression patterns of *doc1, eya,* and *dpp* at ectodermal segmentation stage (24 hpl).

A-B. Enrichment patterns of *doc1* and *dpp* mRNAs at 24 hpl. C-D. Enrichment patterns of *eya* and *dpp* mRNAs at 24 hpl. A-C. maximum intensity projections of embryos. D Projection of internal layers of the embryo in C. Arrowheads in A-D indicate the extend of spread of *dpp* mRNA dorsally. Orange arrowheads in A-B indicate the anterior end of the band of *doc1* along the dorsal midline. Arrows in A-B indicate the posterior end of the band of *doc1* along the dorsal midline. Arrows in C-D indicate the ectodermal layer, which is not enriched for *eya*. Orange arrowheads in C-D indicate the region of the PGCs, which is enriched for *eya*. Left ventrolateral view in A. Right dorsolateral view in B. Dorsal view in C-D. Scale bar = 10 μm.

Figure 9 Summary of BMP and FGF pathway gene expression patterns in *H. exemplaris* embryos between elongation and segmentation stages.

Drawings representative of expression patterns of (A) FGF and (B) BMP signaling pathways in *H. exemplaris* embryos at elongation, endomesodermal pouch formation (E.P.), and ectodermal segmentation (E.S.) stages, shown from lateral and ventral views. From top to bottom, images show surface to internal views (and dorsal surface for ventral views). Anterior (A) is up and Posterior (P) is down in all drawings. Dorsal (D) and (V) are to the left and right, respectively, in the lateral views. Representative summaries of expression patterns are shown as follows: in the top embryos (A), *fgf8* in green, *fgfrl1* in magenta; in the bottom embryos (B), *dpp* in green, *sog* in magenta, *tld* in orange.

Supplementary Figure 1 Identification of an FGF8 homolog in *H. exemplaris*

Above: Maximum Likelihood phylogenetic reconstruction of FGF8 and related amino acid sequences. Branch support out of 100 is given at each node. *H. exemplaris* sequences are highlighted. Protein families are indicated by colored bars to the right of the tree. Deuterostom = Deuterostomes. Below: Alignment used for phylogenetic reconstruction from conserved domain among FGF homologs from several species.

Supplementary Figure 2 Identification of FGF Receptor homologs in *H. exemplaris*

Above: Maximum Likelihood phylogenetic reconstruction of FGF receptors and related amino acid sequences. Branch support out of 100 is given at each node. *H. exemplaris* sequences are highlighted. Protein families are indicated by colored bars to the right of the tree. Cnid = Cnidaria; Loph. = Lophotrocozoa; Deutero = Deuterostomes. Below: Alignment used for phylogenetic reconstruction from conserved domain among FGF receptor homologs from several species.

Supplementary Figure 3 Identification of a Snail homolog in *H. exemplaris*

Above: Maximum Likelihood phylogenetic reconstruction of Snail and related amino acid sequences. Branch support out of 100 is given at each node. *H. exemplaris* sequences are highlighted. Protein families are indicated by colored bars to the right of the tree. Deutero = Deuterostomes. Below: Alignment used for phylogenetic reconstruction from conserved region among Snail homologs from several species.

Supplementary Figure 4 Identification of BMP ligand homologs in *H. exemplaris*

Above: Maximum Likelihood phylogenetic reconstruction of BMP ligands and related amino acid sequences. Branch support out of 100 is given at each node. *H. exemplaris* sequences are highlighted. Protein families are indicated by colored bars to the right of the tree. Below: Alignment used for phylogenetic reconstruction from conserved domain among BMP homologs from several species.

Supplementary Figure 5 Identification of a Sog homolog in *H. exemplaris*

Above: Maximum Likelihood phylogenetic reconstruction of Sog/Chordin and related amino acid sequences. Branch support out of 100 is given at each node. *H. exemplaris* sequences are highlighted. Protein families are indicated by colored bars to the right of the tree. Deuterostom = Deuterostomes. Below: Alignment used for phylogenetic reconstruction from conserved region among Sog/Chordin homologs from several species.

Supplementary Figure 6 Identification of BMP Type I and II Receptor homologs in *H. exemplaris*

Above: Maximum Likelihood phylogenetic reconstruction of BMP receptors Type 1 and 2 and related amino acid sequences. Branch support out of 100 is given at each node. *H. exemplaris* sequences are highlighted. Protein families are indicated by colored bars to

the right of the tree. Below: Alignment used for phylogenetic reconstruction from conserved domain among BMP receptor homologs from several species.

Supplementary Figure 7 Identification of a Tolloid homolog in *H. exemplaris*

Above: Maximum Likelihood phylogenetic reconstruction of Tolloid and related amino acid sequences. Branch support out of 100 is given at each node. *H. exemplaris* sequences are highlighted. Protein families are indicated by colored bars to the right of the tree. Deuterost = Deuterostomes. Below: Alignment used for phylogenetic reconstruction from conserved domain among Tolloid homologs from several species.

Supplementary Figure 8 Identification of a Doc1 homolog in *H. exemplaris*

Above: Maximum Likelihood phylogenetic reconstruction of Dorsocross (Doc) and Optimer Blind (Omb) and related amino acid sequences. Branch support out of 100 is given at each node. *H. exemplaris* sequences are highlighted. Protein families are indicated by colored bars to the right of the tree. Below: Alignment used for phylogenetic reconstruction from conserved domain among Dorsocross homologs from several species.

Supplementary Figure 9 Identification of an Eya homolog in *H. exemplaris*

Above: Maximum Likelihood phylogenetic reconstruction of Eyes absent (Eya) and related amino acid sequences. Branch support out of 100 is given at each node. *H. exemplaris* sequences are highlighted. Protein families are indicated by colored bars to the right of the tree. Deuterost = Deuterostomes. Below: Alignment used for phylogenetic reconstruction from conserved region among Eya homologs from several species.

Supplementary Figure 10 Expression patterns of *fgf8* and *fgfrl1* mRNAs at elongation stage (18 hpl).

A-C. Enrichment patterns of *fgf8* and *fgfrl1* mRNAs at 18 hpl. A. maximum intensity projection of embryo from a dorsolateral view. B. Projection of uppermost layers of the embryo in A. C. Projection of internal layers of the embryo in A. Region outlined with a dashed line indicates the region with signal in the upper layers projected in B, which are omitted in the internal layers projected in C. Arrowheads indicate ectodermal patches of *fgf8* signal. Left dorsolateral view. Scale bar = 10 μm.

Supplementary Figure 11 Expression patterns of *tkv* and *punt* at ectodermal segmentation stage (24 hpl).

A-B. Enrichment pattern of *tkv* mRNAs at 19 hpl (A) and 24 hpl (B) by FISH. C-D. Enrichment pattern of *punt* mRNAs at 19 hpl (A) and 24 hpl (B) by FISH. All images are maximum intensity projections. Embryos are all in ventral or dorsal view, as indicated. Scale bar = 10 μm.

Supplementary Figure 12 Expression patterns of *gbb* and *sog* at ectodermal segmentation stage (24 hpl).

A-D. Enrichment patterns of *gbb* and *sog* mRNAs at 24 hpl. A and C Maximum intensity projections of embryos from a dorsal (A) and lateral (C) view. B. Projection of internal layers of the embryo in A. D. Projection of internal layers of the embryo in C. Arrowheads in A-B indicate region of the PGCs, which is not enriched for *gbb*. Arrows in A-B indicate bands of cells enriched for *sog* on either side of the developing mouth. Asterisks in A-B indicate the hollow space within the developing foregut, which is not enriched for *sog* in its epithelium, but which does contain *gbb* signal. Dorsal view in A-B. Right lateral view in C-D. Scale bar = 10 μm.

Videos

Video 1 Embryo stained for *fgf8* and *fgfrl1* mRNAs at ectodermal segmentation (24 hpl) rotating about the dorsal-ventral axis.

Video curated using FIJI function: stack 3-D projection with interpolation. Annotated in Adobe Premier Pro. Arrow indicates enriched signal for *fgf8* mRNA in ectoderm. Arrowhead indicates enriched signal for *fgfrl1* mRNA in a layer more internal to the enrichment for *fgf8* mRNA. Slices are 0.364 μm in thickness. Scale bar = 10 μm.

Video 2 Embryo stained for *fgf8* and *fgfrl1* mRNAs at ectodermal segmentation (24 hpl) scrolling through z planes in 3-D.

Top right quadrant shows DAPI signal, top left quadrant shows *fgf8* mRNA signal, bottom left quadrant shows *fgfrl1* mRNA signal, and bottom right quadrant shows an overlay of all three channels. Video curated using Zen Black export function of AVI video of split channels. Annotated in Adobe Premier Pro. Slices are 0.144 μm in thickness.

Video 3 Embryo stained for *dpp* and *sog* mRNAs at ectodermal segmentation (24 hpl) rotating about the left-right axis.

Video curated using FIJI function: stack 3-D projection with interpolation. Annotated in Adobe Premier Pro. Arrow indicates absence of signal for either *dpp* or *sog* mRNA in

dorsal-most ectoderm. Arrowheads indicate dorsal-most signal for *dpp* mRNA, which extends further dorsally than does *sog* mRNA. Slices are 0.397 μm in thickness.

Video 4 Embryo stained for *dpp* and *sog* mRNAs at ectodermal segmentation (24 hpl) scrolling through z planes in 3-D.

Top right quadrant shows DAPI signal, top left quadrant shows *dpp* mRNA signal, bottom left quadrant shows *sog* mRNA signal, and bottom right quadrant shows an overlay of all three channels. Video curated using Zen Black export function of AVI video of split channels. Annotated in Adobe Premier Pro. Slices are 0.397 μm in thickness.

Figure 1

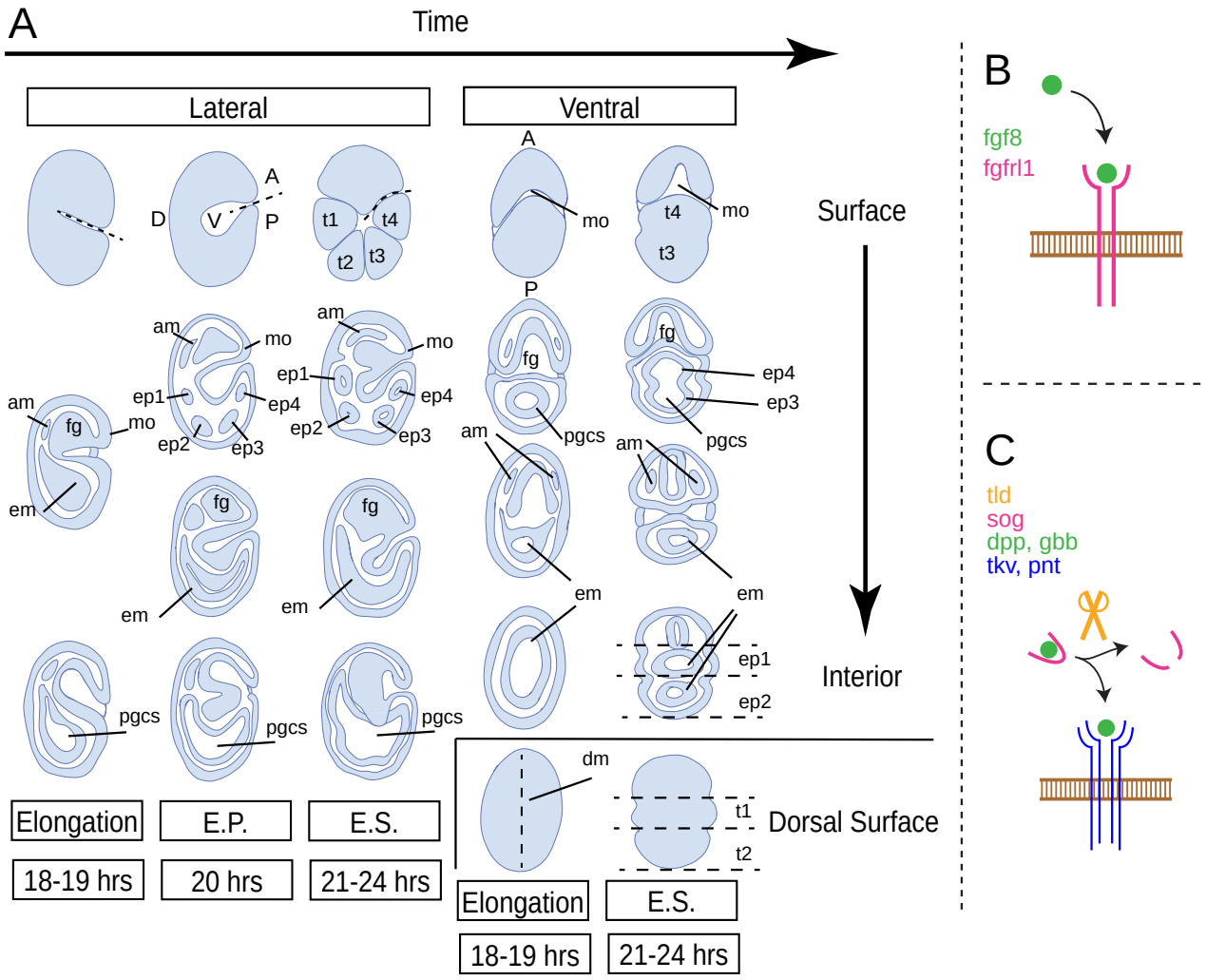

Figure 2

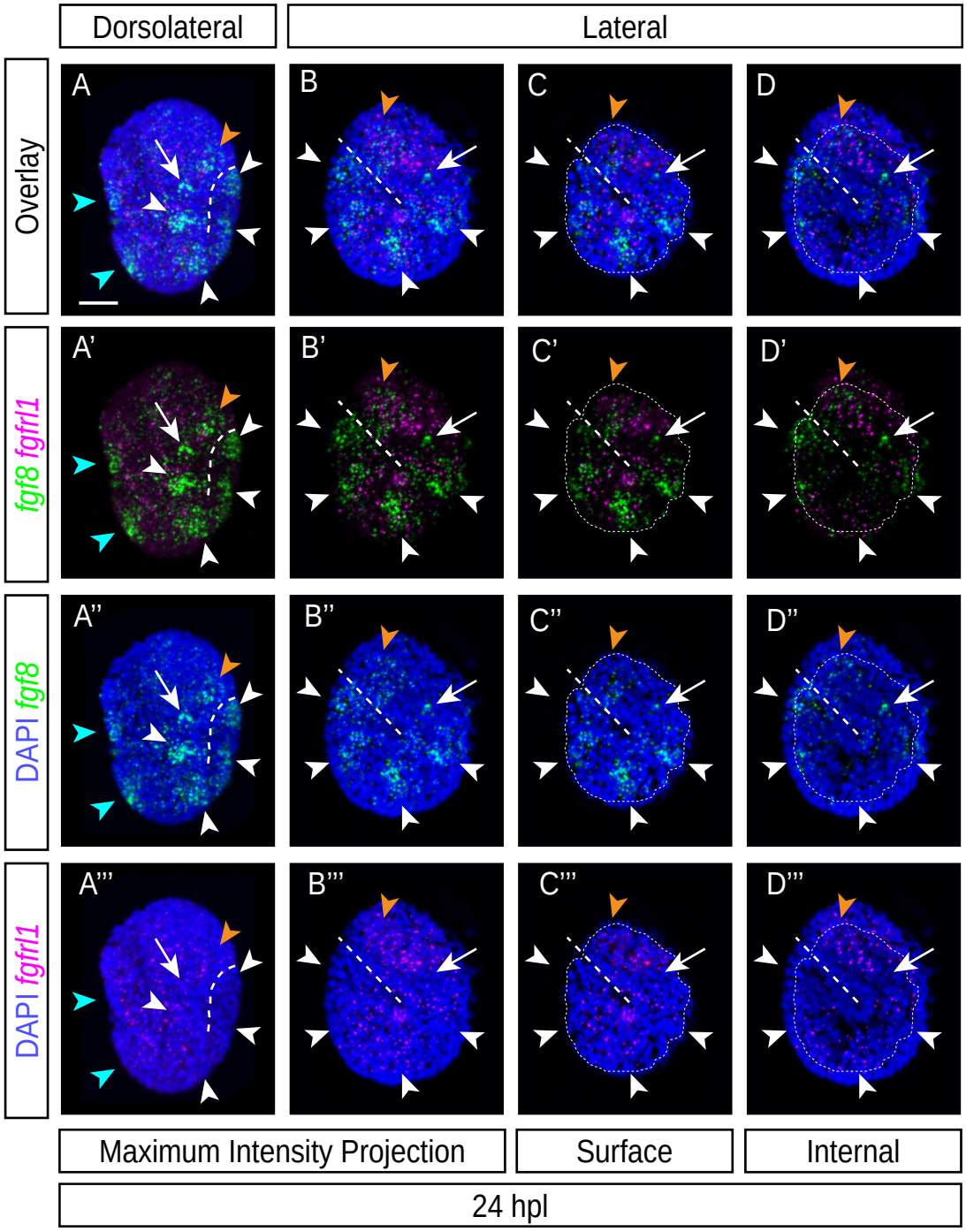

Figure 3

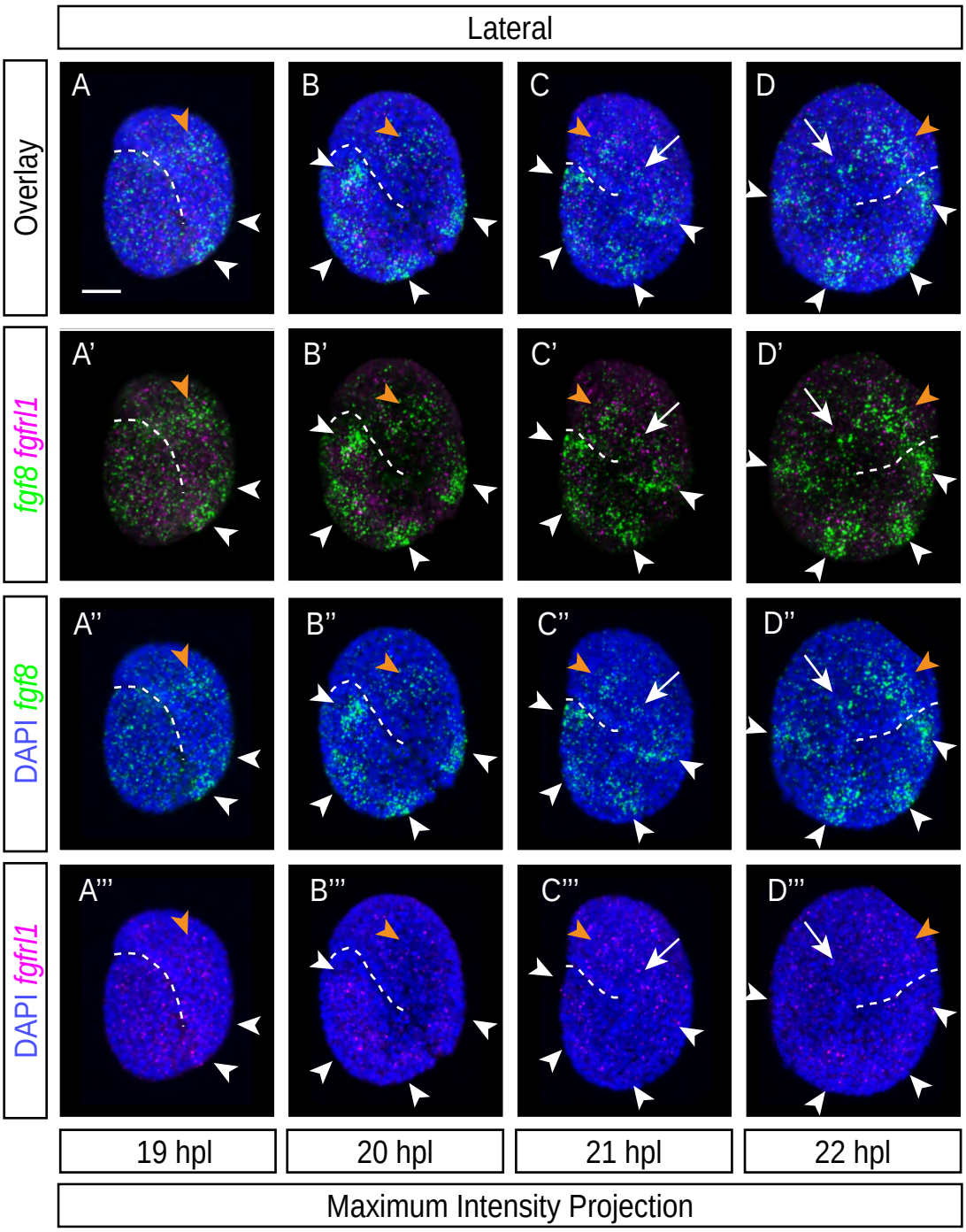

Figure 4

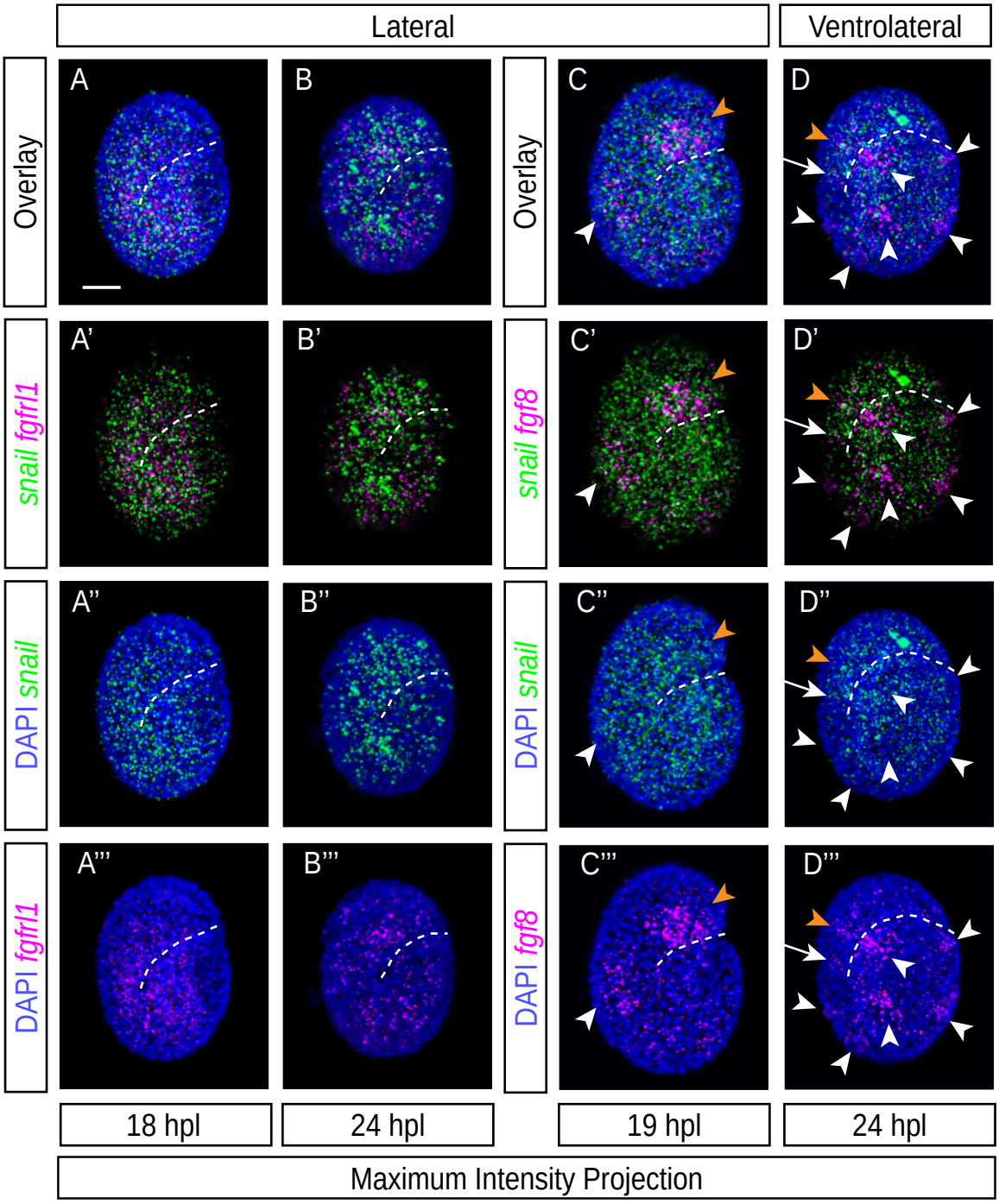

Figure 5

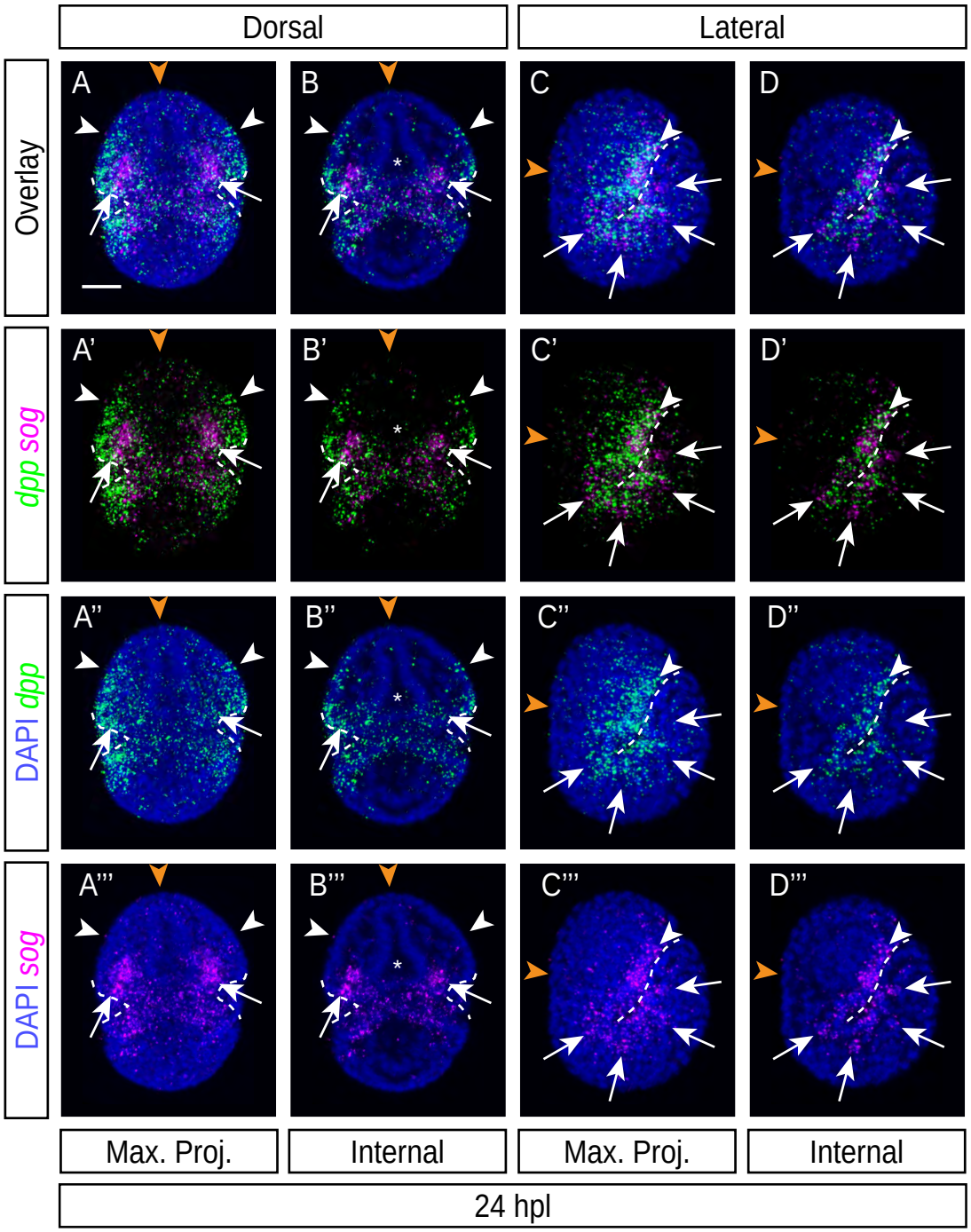

Figure 6

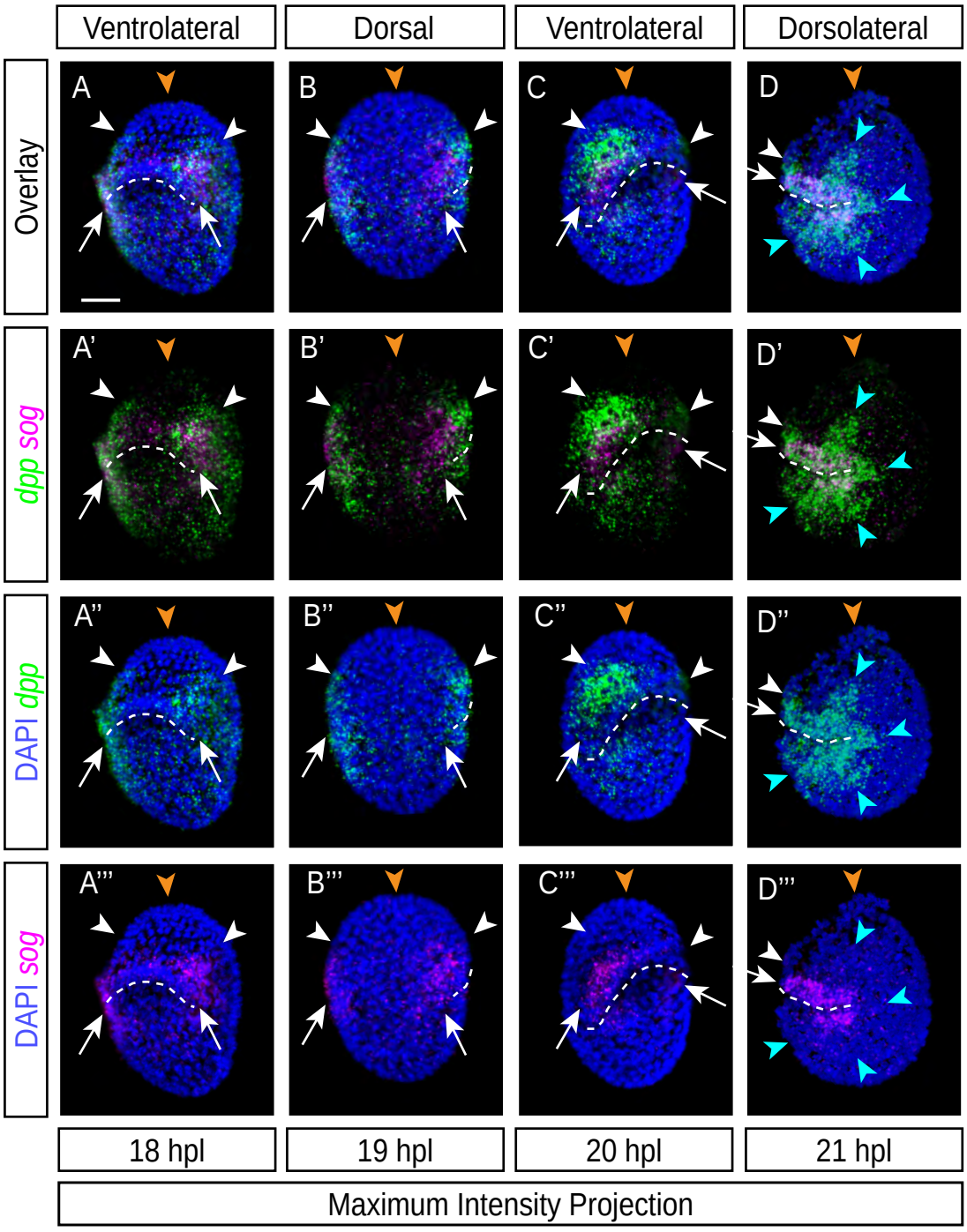

Figure 7

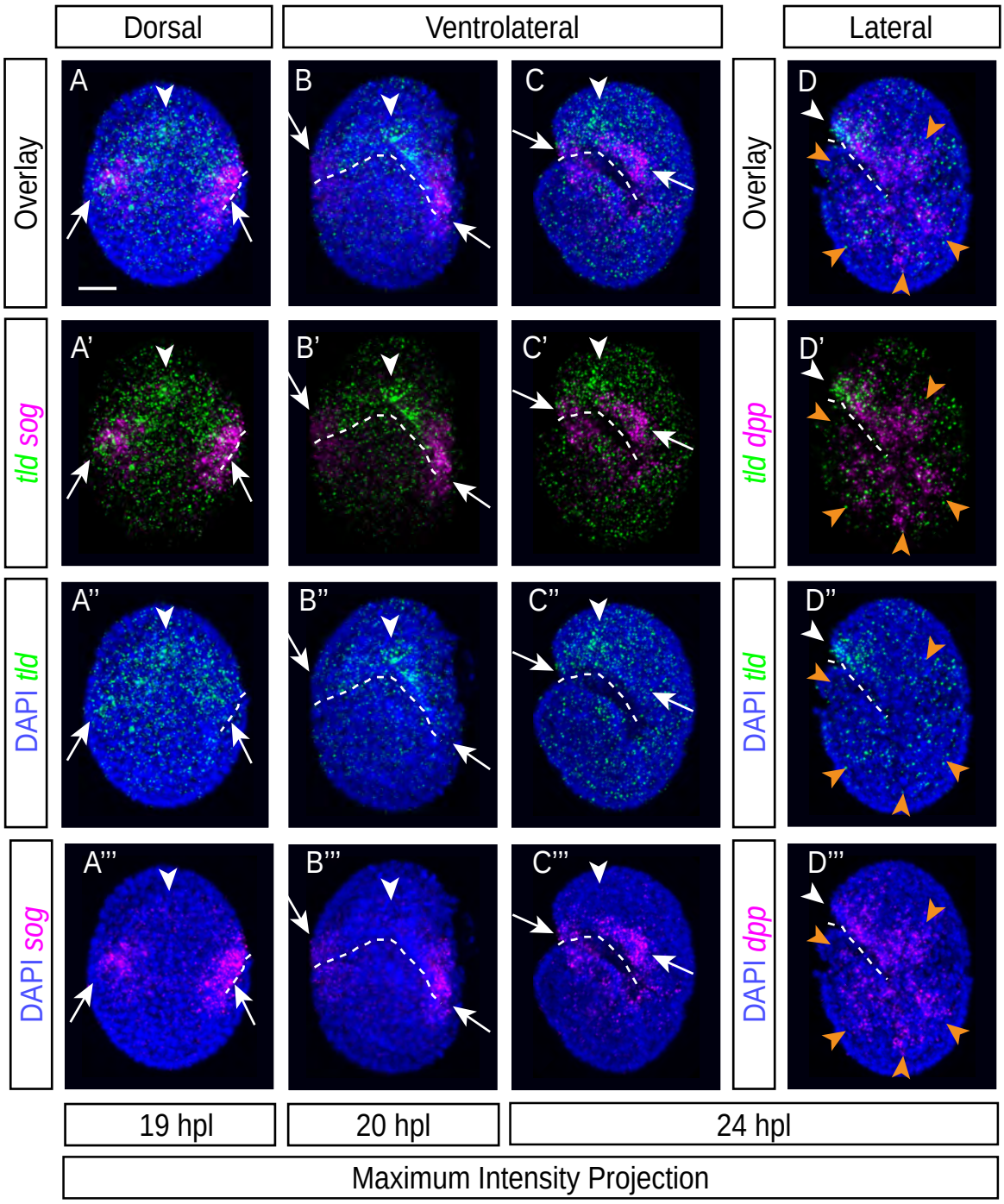

Figure 8

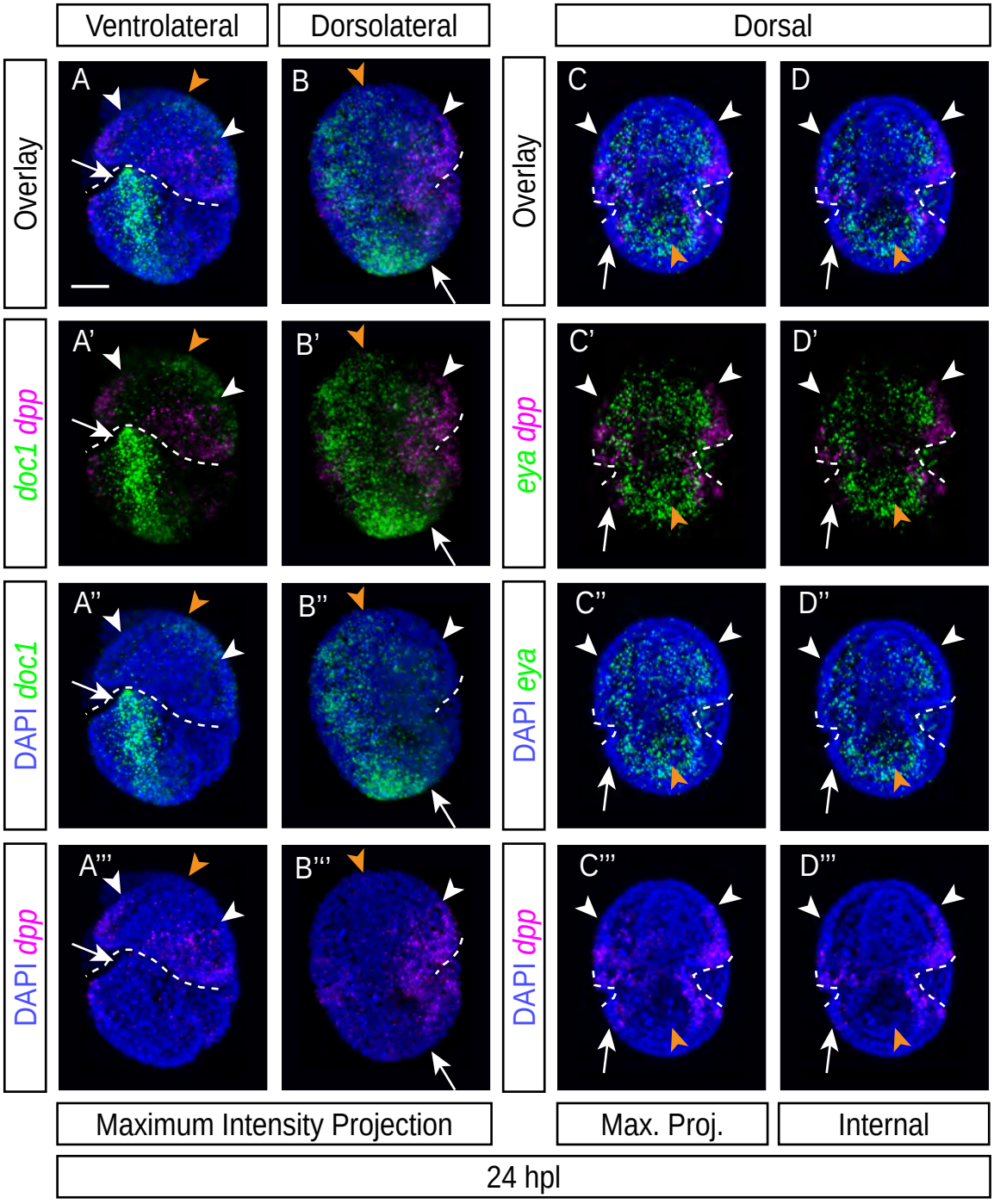

Figure 9